Physics Engineering
Final thesis work

Photonic correlators for passive imaging using synthetic aperture radiometry in the microwave band

Ivan Zhou

Supervised by Dr. Maria C. Santos

Presented on date 30^{th} $January$ 2019

Registered at

Escola Tècnica Superior d'Enginyeria de Telecomunicació de Barcelona

UNIVERSITAT POLITÈCNICA DE CATALUNYA BARCELONATECH

Acknowledgements

I would like to express my gratitude to my thesis director, Dr. Maria C. Santos, for her patience and support during this work. I also want to thank Dani Nuño for his constant help during these months.

Thanks to my family and my friends for your constant support.

Finally, I would like to thank a very special person, thank you Rosalí.

CONTENTS

List of abbreviations used along the thesis :

Abbreviation	Meaning
em	Electromagnetic
SA	Synthetic aperture
SAR	Synthetic aperture radiometer
TPR	Total power radiometer
EOM	Electrooptic modulator
PM	Phase modulator
USB	Upper sideband
USBs	Upper sidebands
LSB	Lower sideband
LSBs	Lower sidebands
FOV	Field of view
DFB	Distributed feedback
RF	Radiofrequency
SMOS	Soil moisture ocean salinity
CCD	Charge couple device
AF	Array Factor

1.Introduction

Life is all about communicating and interacting with our surroundings. Our brain is continuously processing the information provided by our senses to decide which actions to take. This information is vital, it tells us to wait to drink that very hot cup of coffee, to step out of the way of a fast approaching car, etc. Taken to a larger scale, the more information we may gather from our environment, the better will we be able to control and master it, and to make appropriate decisions that may improve the life conditions in our planet. This is what sensing is all about.

Electromagnetic (em) waves are very convenient carriers of environmental information. In the optical visible band, em waves bouncing off from objects are detected by our eyes to tell us about colors, shapes, textures ... but there's certainly more to em wave sensing that meets the eye. An interesting band is the microwave band ranging from 1-300GHz, it not only allows sensing in hostile conditions such as darkness, fog, etc, it also allows to penetrate opaque objects such as clouds, ground, some textiles, etc. With suitable designed sensors, it is thus possible to infer information about surface geometry as well as the electrical properties of the substances, complementing the information obtained from visible and infrared radiation, facilitating studies of geometric, bulk-dielectric, and molecular resonance properties of a surface feature.

Microwave sensing may be either passive or active. Passive systems, known as radiometers, aim at measuring the natural thermal radiation from a body, while active systems, known as radars, differ from radiometers in that they include a transmitter and they detect the wave reflected from the target. Because they are low-power and maintenance, passive systems are preferred for applications such as Earth Observation. Also because of health concerns, they are the most popular choice for security screening of people.

Even when most of the results in this thesis could be valid for other applications, here we focus on Earth Observations using passive radiometers. The connection of the measured emissivity with the object properties is out of our scope. For an in-depth refer to [1].

Radiometers can be classified in two main groups depending on their antenna configuration. One is the real aperture radiometers, i. e. the Total Power Radiometer (TPR), which consists in a single large antenna to receive the electromagnetic radiation coming from a scene. The other group is composed by synthetic aperture Radiometer (SAR) , consisting on an array of antennas that simulates an effective large aperture. There are two main problems for a real aperture antenna. One is that the angular resolution of this system is limited by classical diffraction theory. Assuming radiation at wavelength λ and a circular aperture of diameter D the diffraction-limited angular resolution in radians is given by $\Delta\theta = 1.22\frac{\lambda}{D}$. For example, to obtain resolution of 10 km at 2 GHz would require an aperture of more than 14 meters in a low earth orbit with an 800 km altitude, which makes the design bulky and heavy. Also, mapping of the scene of radiation requires scanning methods (e.g cross track, conical, push-broom) or

multiple beams, because one snapshot of this kind of radiometers only provides data from a single point increasing the time for mapping the whole scene.

These problems can be overcome in a SAR. At the cost of increasing its complexity, the resolution of the image is highly enhanced as it is defined by the maximum separation of antennas rather than the individual antenna size. The image of the scene is retrieved by an inverse Fourier transform of the correlations between each pair of antennas (called baselines). An example of using this technology is the Moisture and Ocean Salinity (SMOS) mission launched on 2 November 2009, which is a satellite aimed to provide global volumetric soil moisture and ocean salinity. See Figure 1.1 and [2]

Figure 1.1 View of SMOS satellite. The SAR called MIRAS for Microwave Radiometer with Aperture Synthesis, is composed by 69 antennas on a Y shaped deployable platform.

For a non-redundant N element interferometric imaging array, there are in total $N(N-1)/2$ independent baselines and the same number of correlations are needed, which results in a high demand for data processing as the number of receives increases. Photonic correlation SA radiometers are thus proposed to exploit the advantages that photonic techniques provide such as high bandwidth, no em interferences, low loss, low weight, high flexibility etc.

The first proposal of using photonics for the correlations and image retrieving dates back to 1999 by Blanchard [3]. This image is formed by upconverting the RF signals in the optical domain by means of electrooptic modulators, and transporting it by optical fibers to a lens where they are interfered in such a way that by square rule of each quadratic detector from the CCD camera the correlations and Fourier transform are achieved.

However, the coherence between each channel has to be maintained which is difficult at optical frequencies because little variations of the temperature, vibrations in the fiber introduce a random phase that breaks the coherence. Blanchard proposes a feedback loop system which compensates this phase error from each channel in real time. Recent works taking off from Blanchard's idea are for example [4] and [5]. All of them incorporate the phase error compensation technique with the disadvantage that fast phase error changes may not be fixed fast enough. In 2015 E.Nova in his doctoral thesis, carried out his investigations on a system that avoids this feedback loop system by using waveguides instead of optical fibers. He worked on the advantadges of photonics in signal distribution but keeping the correlations and image reconstruction in the

microwave domain. An important drawback is that expensive custom integrated photonics would be required for a large array.

In this thesis we present a work on a proposal which consists in doing the correlations in the optical domain by using a remodulation technique where the phase error is avoided so neither feedback loop is needed nor waveguides.

1- Review of the basic theory behind the synthetic aperture radiometers

2- Study of photonic correlators.

2.1 Assessments of advantages and challenges regarding use of photonics in Synthetic Aperture Radiometers.

2.2 Review of ongoing works

3- Description of new photonic correlation system proposals

3.1 Theoretical Analysis

3.2 Validation through both simulations and experiments.

2.Summary

The first part of our work consists in the modeling of the natural emission from bodies

Next, two techniques using passive radiometry are presented. First the simpler one which is the Total Power Radiometer (TPR) is introduced, followed by a more complex technique for which our photonic correlator is designed, the Synthetic Aperture Radiometer (SAR) for passive imaging. Then, general parameters of the SAR such as the sensitivity, angular resolution and field of view (FoV) are presented. We are going to see that all those parameters are related and need to be taken into account when designing a correlator.

The major drawback of a photonic correlator is to maintain coherence between each channel as described in 1, several ongoing works trying to fix this problem, [3], [5] and [6] are discussed.

And finally, we present our novel technique which doesn't depend on this phase error, reducing complexity of electronics and making the setup robust by avoiding feedback compensation loop. Simulations and experimental setup that validates the theory of the design are successfully carried out and shown.

We will show that our setup is limited by effect of the so called fringe washing function which decorrelates our correlations. A final solution doubling the number of electro-optical modulators is proposed in order to improve it.

3. Earth observation fundamentals

In this chapter, some of the fundamental properties of earth radiation are introduced with the main purpose of understanding the selection of the frequencies adopted by radiometers when observing the Earth .

3.1 The electromagnetic spectrum

The principal band where satellites for Earth observation works is the microwave band ranging from 1GHz to 300GHz. Figure 3.1 shows the atmospheric transmissivity in this frequency range.

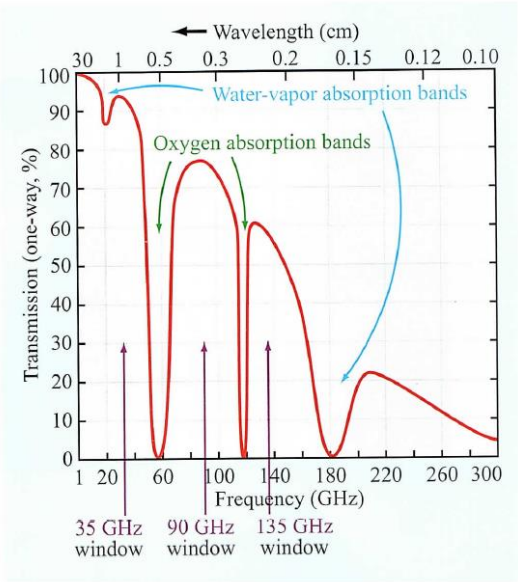

Figure 3.1 Atmospheric transmissivity of Earth in the microwave domain from [1].

Atmospheric opacity and transmissivity play a key role in frequency selection for remote sensing, within or through the atmosphere. For example, because of water-vapor absorption near 58 and 119GHz, these frequencies are used almost exclusively for radiometric observations of the atmosphere. In contrast, because at frequencies below 20GHz the atmosphere is essentially transparent, and in atmospheric “windows” signal attenuation is tolerable, sensors observing the Earth’s surface through the atmosphere are operated at frequencies below 20GHz and at those within the transmission windows shown in 3.1. For example in SMOS uses 1.41 GHz because H_2O vapour radiation comes from this band or short range radar applications such as vehicle anti-collision radars operate at 77GHz where atmospheric attenuation helps minimize interference from distant radars.

3.2 Natural Radiation from bodies

In this section , natural radiation is studied and modeled. It is very important because depending on the level of this radiation some properties of the materials can be measured.

3.2.1 Black body : Planck's law

A blackbody is an idealized body that, when in thermodynamic equilibrium at a temperature T_{ph}, radiates at least as much energy as any other body at the same temperature and it's also a perfect absorber.

The spectral brightness B_b is defined for an extended black body source as the radiated power density, per unit frequency per stereo radian of black-body as seen from an observation point, see figure 3.3 at a physical temperature T_{ph} and it is quantified by the Planck's law:

$$B_b = \frac{2hf^3}{c^2}\frac{1}{e^{\frac{hf}{K_B T_{ph}}-1}} \qquad [Wm^{-2}sr^{-1}Hz^{-1}] \qquad (3.1)$$

here h is the Planck's constant, K_B is the Boltzmann constant, f is the radiation frequency and c is the speed of light. If $f \ll 6THz$ for a blackbody of $T_{ph} = 300K$, the exponential function dividing the Planck's law can be approximated by a first order Taylor:

$$e^{\frac{hf}{K_B T_{ph}}} - 1 \approx \frac{hf}{K_B T_{ph}}$$

Yielding the Rayleigh Jean's law:

$$B_b = \frac{2K_B f^2}{c^2} T_{ph} \qquad [Wm^{-2}sr^{-1}Hz^{-1}] \qquad (3.2)$$

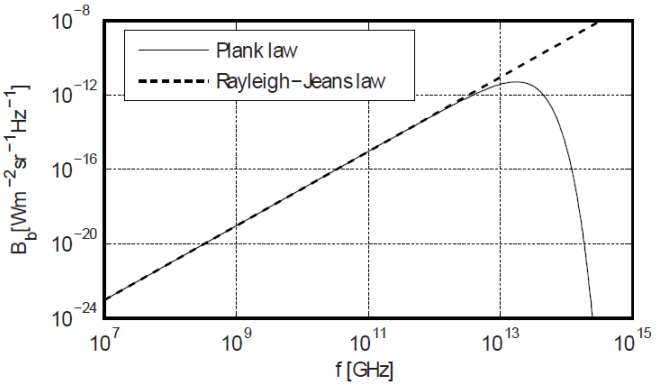

Figure 3.2 Spectral brightness B_b of a black-body with a physical temperature $T_{ph} = 300K$ calculated using the Planck's law and the Rayleigh-Jeans approximation from [7]

3.2.2 Gray body

Real sources, sometimes referred to as gray bodies, emit less than a blackbody does and do not necessarily absorb all the energy incident upon them. In addition, its brightness function at every point of the extended gray source may be direction dependent as:

$$B_g(\theta,\phi) = \frac{2K_B f^2}{c^2} T_B(\theta,\phi) = B_b\, e(\theta,\phi) \tag{3.3}$$

Where θ and ϕ are elevation and azimuth angles as seen from a specific point of the gray body, $T_B(\theta,\phi)$ and $e(\theta,\phi)$ are defined respectively as the body's brightness temperature , and emissivity . They are related through the body's physical temperature as:

$$e(\theta,\phi) = \frac{T_B(\theta,\phi)}{T_{ph}} \tag{3.4}$$

3.3 Radiation produced by Earth

The Earth is an extended gray body source which emits random electromagnetic radiation with equal probability for horizontal and vertical polarization. Since antennas are only sensitive to one polarization the expression of the field as detected by the antenna can be modelled as a scalar field $x(\bar{r},t)$ with $\bar{r} = (x,y,z)$ satisfying the scalar wave equation:

$$\nabla^2 x - \frac{1}{c^2}\frac{\partial^2 x}{\partial t^2} = 0 \tag{3.5}$$

Where c is the velocity of the light $3\ 10^8 m\ s^{-1}$ and ∇ is the Laplacian operator.

In an elementary view, $x(\bar{r},t)$ is the instantaneous amplitude of the transverse electric field in the antenna's direction of polarization.

$x(\bar{r},t)$ also can be described in the Fourier domain :

$$X(\bar{r},f) = \mathcal{F}(x(\bar{r},t)\,) = \int_{-\infty}^{\infty} x(\bar{r},t) e^{-j2\pi f t} dt \tag{3.6}$$

$$x(\bar{r},t) = \mathcal{F}^{-1}\big(X(\bar{r},f)\big) = \int_{-\infty}^{\infty} X(\bar{r},f) e^{j2\pi f t} df \tag{3.7}$$

With (3.6) and (3.7) in (3.5) the frequency wave equation is obtained :

$$\nabla^2 X(\bar{r},f) + k^2 X(\bar{r},f) = 0 \tag{3.8}$$

Where $k = \frac{2\pi f}{c}$ is the wavenumber. Solving this equation for a point source from $\bar{r}_i = (x_i, y_i, z_i)$, the spectral amplitude at the antenna at point $\bar{r}_1 = (x_1, y_1, z_1)$:

$$X(\bar{r}_i, f) = \frac{A(\bar{r}_i, f)}{r_{1i}} e^{-jkr_{1i}} \tag{3.9}$$

r_{1i} being the distance between source point i and point 1. We can also see that now $A(\bar{r}_i, f)$ is a complex function of frequency.

In the time domain one has :

$$x(\bar{r}_i, t) = \int_{-\infty}^{\infty} \frac{A(\bar{r}_i, f)}{r_{1i}} e^{-jkr_{1i}} e^{j2\pi ft} df = \frac{a\left(t - \frac{r_{1i}}{c}\right)}{r_{1i}} \tag{3.10}$$

The power density radiated by the gray body before being captured by the antenna is the double as all polarizations have to be taken into account. The spectral amplitude of the field, the modulus of the Poynting vector per unit frequency, $P_r(\bar{r}_i, f)$ and the spectral brightness of the body are related as follows :

$$P_r(\bar{r}_i, f) = \frac{2|X(\bar{r}_i, f)|^2}{\eta_0} = B_g(\theta_i, \phi_i)\Delta\Omega \qquad [W\, m^{-2}\, Hz^{-1}] \tag{3.11}$$

The modulus of Poynting vector per unit frequency is the spectral brightness radiated by an amount of solid angle $\Delta\Omega$ of the point source as seen from the observation point, see Figure 3.3.

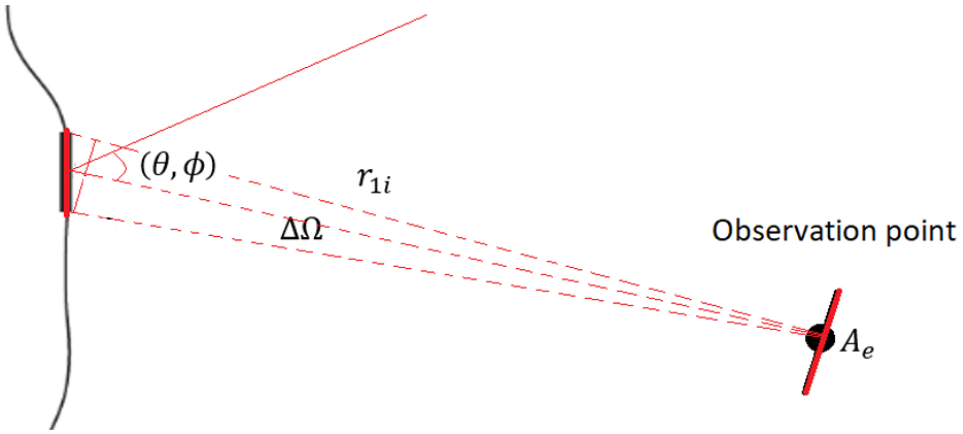

Figure 3.3 Scheme showing the elevation and azimuth angles (θ,ϕ) seen from the source "point" and the solid angle, as seen from the observation point.

The spectral power density collected by the antenna would be just multiplying (3.11) by the effective area of the antenna and dividing by 2:

$$P(f, \theta_i, \phi_i) = \frac{|X(\bar{r}_i, f)|^2}{\eta_0} A_e(\theta_i, \phi_i) = \frac{1}{2} B_g(\theta_i, \phi_i)\Delta\Omega A_e(\theta_i, \phi_i) \quad \left[\frac{W}{Hz}\right] \tag{3.12}$$

Remember that only half of the polarization is captured by the antenna, hence half of the power radiated is received.

3.4 Power received from a gray body source

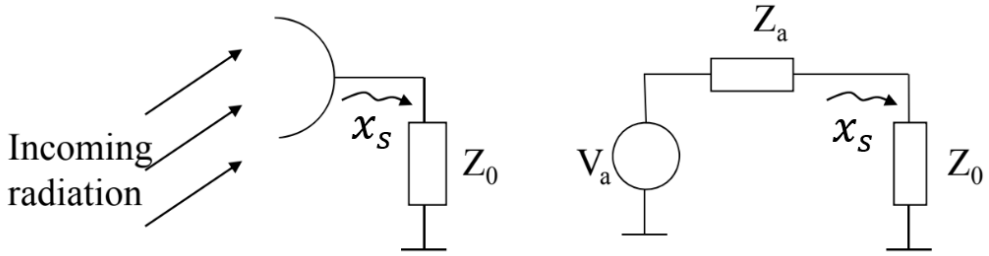

Figure 3.4 Left : receiving antenna connected to a reference impedance Z_0. Right: the equivalent circuit model taking into account the antenna.

The normalized open circuit voltage generated by the antenna with an incident electrical wave $x(\bar{r}_i, t)$ from the point source polarized in the direction of the antenna's polarization is:

$$V_a(\bar{r}_i, t) = \frac{x_l(\bar{r}_i, t)}{\sqrt{Z_0}} \tag{3.13}$$

where Z_0 is the load impedance and $x_l(\bar{r}_i, t)$ is the incident electrical wave taking into account the response of the antenna, that is the effective length defined in the frequency domain as:

$$l_e(\theta_i, \phi_i) = \sqrt{\frac{4R_a A_e(\theta_i, \phi_i)}{\eta_0}} \tag{3.14}$$

And the spectral component of $x_l(\bar{r}_i, t)$ is:

$$X_l(\bar{r}_i, f) = X(\bar{r}_i, f) l_e(\theta_i, \phi_i) \tag{3.15}$$

Where $R_a = Re(Z_a)$ is the real part of the antenna impedance and η_0 is the free space impedance. The maximum power transferred to the load impedance Z_0(usually 50Ω) occurs when they are matched ($Z_0 = Z_a^*$). Assuming real antenna impedance such that $Z_0 = R_a$, the voltage x_s (see figure 3.4) is just half the open circuit voltage:

$$x_s(\bar{r}_i, t) = V_a(\bar{r}_i, t) \ \frac{Z_0}{Z_0 + Z_a} = V_a(\bar{r}_i, t) \ \frac{1 + \Gamma_a}{2} = \frac{x_l(\bar{r}_i, t)}{2\sqrt{R_a}} \tag{3.16}$$

Note that $\Gamma_a = \frac{Z_a - Z_0}{Z_0 + Z_a}$ is the reflection coefficient assumed 0 here.

Taking into account the receiver response which usually is a band pass filter and an amplifier $h(t) = \sqrt{G}\, \mathcal{F}^{-1}\left(\prod(\frac{f - f_0}{B} + \frac{B+1}{2})\right)$:

$$x_r(\bar{r}_i, t) = x_s(\bar{r}_i, t) * h(t) = \frac{x_l(\bar{r}_i, t) * h(t)}{2\sqrt{R_a}} \tag{3.17}$$

The instantaneous power delivered to the reference impedance coming from the extended source is for a matched impedance :

$$P(t) = \overline{|x_r(\bar{r}_\iota, t)|^2} = \frac{\overline{|x_l(\bar{r}_\iota, t) * h(t)|^2}}{4\, R_a} \tag{3.18}$$

Where the bar " $\bar{}$ " notation denotes the contribution from all the points of the extended source, that is, integrated over the gray body solid angle seen from the antenna position.

The average of this power is, by Parseval's theorem :

$$P_a = \lim_{T\to\infty} \frac{1}{T} \int_{-\frac{T}{2}}^{\frac{T}{2}} \overline{|x_r(\bar{r}_\iota, t)|^2}\, dt = \int_{-\infty}^{+\infty} \overline{|X_r(\bar{r}_\iota, f)|^2}\, df = \int_{-\infty}^{\infty} \frac{\overline{|X(\bar{r}_1, f)|^2 A_e(\theta_\iota, \phi_\iota)}}{\eta_0} |H(f)|^2 df \tag{3.19}$$

where $A_e(\theta, \phi) = \frac{\lambda^2 t(\theta,\phi)}{\iint_{4\pi} t(\theta,\phi) d\Omega} = \frac{\lambda^2 t(\theta,\phi)}{\Omega_a}$ is the effective area of the antenna and Ω_a is the antenna solid angle. (3.20)

The term $\frac{\overline{|X(\bar{r}_1, f)|^2 A_e(\theta_i, \phi_i)}}{\eta_0}$, by using (3.12) becomes:

$$\frac{\overline{|X(\bar{r}_1, f)|^2 A_e(\theta_\iota, \phi_\iota)}}{\eta_0} = \frac{1}{\Omega_a} \iint_{Source} \frac{B_g(\theta,\phi)}{2} \lambda^2 t(\theta, \phi)\, \mathrm{d}\Omega = \frac{K_B}{\Omega_a} \iint_{Source} T_B(\theta, \phi) t(\theta, \phi)\, \mathrm{d}\Omega \tag{3.21}$$

The power from the gray body-like source transferred to the impedance is :

$$P_a = \int_{-\infty}^{+\infty} \frac{K_B}{\Omega_a} \iint_{Source} T_B(\theta, \phi) t(\theta, \phi) |H(f)|^2 df\, \mathrm{d}\Omega = G\, K_B B\, T_a \qquad [W] \tag{3.22}$$

Where T_a is known as the antenna temperature :

$$T_a = \frac{1}{\Omega_a} \iint_{Source} T_B(\theta, \phi) t(\theta, \phi)\, \mathrm{d}\Omega \tag{3.23}$$

We should clarify that in this thesis we will neglect the effect of the atmosphere which may mask the brightness temperature, so instead of receiving $T_B(\theta, \phi)$ we would receive an apparent brightness temperature :

$$T_{AP}(\theta, \phi) = T_{UP}(\theta, \phi) + \frac{\left(T_B(\theta,\phi) + T_{SC}(\theta,\phi)\right)}{L_a} \tag{3.24}$$

Where T_{UP} is the atmospheric upward radiation, T_{SC} is the downward atmospheric radiation scattered by the Earth in the direction of the antenna, and L_a represents the atmosphere attenuation. For more details refer to [1].

4. Passive Microwave Radiometry

In this chapter 2 techniques for passive imaging are discussed. First, the simpler architecture of a passive radiometer, the total power radiometer (TPR) is discussed. Then the synthetic aperture interferometric radiometer is presented.

Our work focuses in this last technique but using photonics in order to assist performing the complex correlations.

4.1 The Total Power Radiometer

A TPR consists in a real aperture antenna that receives the upcoming radiation from a quasi point source, integrated in a certain time τ in order to improve the sensitivity of the system after filtering , amplifying and detecting it with a quadrature response device.

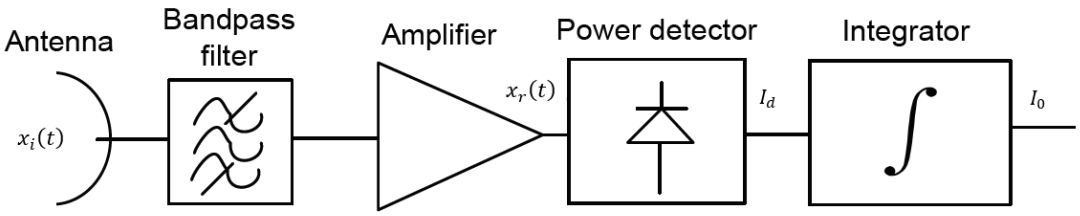

Figure 4.1 Scheme of a receiver chain of the TPR

The signal $x_r(t)$ after filtering at a center frequency ω_m with bandwidth B and amplifying by G, can be modelled as :

$$x_r(t) = Re\big(\, n_i(t)\, e^{j\omega_m t}\,\big) = \, n_{Ii}(t)\cos(\omega_m t) - n_{Qi}(t)\sin(\omega_m t) \qquad (4.1)$$

Where $n_i(t) = n_{Ii}(t) + jn_{Qi}(t)$ is the equivalent baseband noise, with the equivalent phase and quadrature components, $n_{Ii}(t)$ and $n_{Qi}(t)$ respectively.

The detected signal follows the square rule, generating a current proportional to the power of the signal :

$$I_d(t) = x_r^2(t) = \frac{1}{2}\|n_i(t)\|^2 \qquad (4.2)$$

Where is assumed that the square-law detector is a slow-response circuit, so the terms associated with ω_m won't be detected.

The integrator of the radiometer has a constant time τ and current gain g_I. Its output current is :

$$I_o = \frac{g_I}{\tau}\int_{t-\tau}^{t} I_d(t')\, dt' \qquad (4.3)$$

$$If\ B\tau \gg 1$$

$$I_o \approx \frac{1}{2} g_I G K_B T_{sys} B \tag{4.4}$$

Where $T_{sys} = T_a + T_{REC}$. Note that as we are receiving the power from a quasi point source, I_o is the same as (3.22) but taking into account the whole receiver noise T_{REC} and respective gains.

In a TPR the antenna temperature for a target coming from (θ_0, ϕ_0):

$$T_a = \frac{1}{\Omega_a} \iint_{Source} T_B(\theta_0, \phi_0) t(\theta, \phi)\, \mathrm{d}\Omega = \quad T_B(\theta_0, \phi_0) \frac{\iint_{Source} t(\theta, \phi)\, \mathrm{d}\Omega}{\Omega_a} \tag{4.5}$$

With highly directive antennas $\frac{\iint_{Source} t(\theta,\phi)\mathrm{d}\Omega}{\Omega_a} \approx 1$ so the antenna temperature is directly the brightness temperature $T_a = T_B(\theta_0, \phi_0)$. From (4.4) and taking into account (4.5) :

$$T_B(\theta_0, \phi_0) = \frac{I_o}{g_I G K_B B} - T_{REC} \tag{4.6}$$

We can see in (4.6) that there is a linear relation between the unknown brightness temperature $T_B(\theta_0, \phi_0)$ and I_o , so the physical constants of the system can be determined through calibration. If we want to map the whole scene, we need to use scanning methods (e.g. cross track, conical, push-broom) or multiple beams.

4.1.1 Sensitivity of a TPR

Since the integration time τ is finite, the value of $T_B(\theta_0, \phi_0)$ it measures is not the true value of T_B, but rather an estimate of that value with an uncertainty $\Delta T_B(\theta_0, \phi_0)$ That is called the radiometric sensitivity of the system.

If we suppose $n_{Ii}(t)\ and\ n_{Qi}(t)$ respectively, are independent stochastic processes with Gaussian probability density function. After the square rule detector see 4.2, I_d behaves as an exponential pdf form :

$$I_d = E\left\{\frac{1}{2}\|n_i(t)\|^2\right\} = \sigma = \frac{1}{2} g_I G K_B B T_{sys} \tag{4.7}$$

In an exponential pdf, the standard deviation equals the mean value, making the radiometer impractical and useless. The obvious solution to the problem is to filter out the fluctuations of the detected current as done in (4.3), which is equivalent to averaging I_d over some interval of time τ. The standard deviation becomes :

$$std_{integ}(I_o) = \frac{1}{2} g_I G K_B B \Delta T_{sys} = \frac{\sigma}{\sqrt{N}} = \frac{g_I K_B B G T_{sys}}{2\sqrt{B\tau}} \tag{4.8}$$

Where the number of samples taken is $N = B\tau$.

Then from the equation above we can derive the sensitivity of the TPR radiometer [1]:

$$\Delta T_{sys} = \frac{T_{sys}}{\sqrt{B\tau}} \tag{4.9}$$

As we can see, the higher the integration time and bandwidth, the higher sensitivity of the radiometer. The trade-off is a slow response time to changes in the scene.

4.2 Synthetic Aperture Radiometer

The synthetic aperture radiometer is formed by an array of little antennas that synthesizes a large aperture antenna. In order to retrieve the brightness temperature, the cross correlations between all the signals arriving to each pair of antennas (called baselines) are needed. We will see that the inverse Fourier transform of those cross correlations is the modified brightness temperature which is related to the real brightness temperature but taking into account the no idealities of the receivers. Focusing in the simplest case of a SAR correlator:

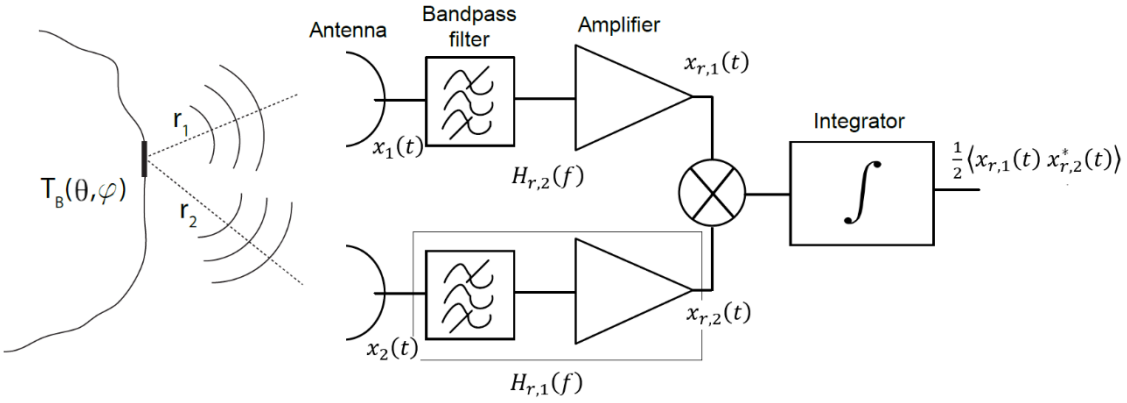

Figure 4.2 Scheme of a pair of receiver chain from a SAR

Here we have 2 antennas of the SAR array which receive the natural radiation from the source. The point source's radiation will arrive to the antenna 1 with a time difference of $+\Delta r_{1-2}/c$ with respect to the second antenna.

The voltage waves from the antennas $x_1(t)$ and $x_2(t)$ are proportional to the upcoming electric field $x(t)$ $[V/m]$ of the source and depend on the effective length of the antenna in the received direction, $l_{e,1}(\theta,\phi)$ and $l_{e,2}(\theta,\phi)$.

As we are dealing with thermal noise signals they have to be filtered in order to fix the coherence time which depends on the inverse of the filter's bandwidth $t_{coh} = 1/B$. For large bandwidths, the correlation of 2 signals with $\Delta r_{1-2}/c \gg t_{coh}$ may loose information and it is irrecoverable. An in-depth discussion on the decorrelation effects will be given later.

After the filtering, the amplification is necessary because in most of the cases, we are

dealing with very weak signals. Finally $x_{r,1}(t)$ and $x_{r,2}(t)$ are correlated by means of a multiplier and integrator.

4.2.1 The visibility function

Assuming stochastic stationary ergodic process, the time domain cross correlation of $x_{r,1}(t)$ and $x_{r,2}(t)$ taking into account an extended source is :

$$R_{x_{r,1}\,x_{r,2}}(0) = \lim_{T\to\infty} \frac{1}{T} \int_{-\frac{T}{2}}^{\frac{T}{2}} \overline{x_{r,1}(\bar{r}_i, t)\; {x_{r,2}}^*(\bar{r}_i, t)}\, dt \tag{4.10}$$

Remember that the bar means the contribution from all the points of the source and the normalized voltage waves from each antenna delivered to each matched reference impedance is, see (3.17) and (3.15):

$$x_{r,1}(\bar{r}_i, t) = \frac{x_1(\bar{r}_i,t) * h_{r,1}(t)}{2\sqrt{R_a}} \;;\; X_1(\bar{r}_i, f) = l_{e,1}(\theta, \phi)\, X(f) \tag{4.11}$$

$$x_{r,2}(\bar{r}_i, t) = \frac{x_2(\bar{r}_i,t) * h_{r,2}(t)}{2\sqrt{R_a}};\; X_2(\bar{r}_i, f) = l_{e,2}(\theta, \phi)\, X(f) e^{\frac{-j2\pi f \Delta r_i}{c}} \tag{4.12}$$

It is important to emphasize that we are assuming incoherent source and that the antennas are close enough so the direction coming from each point source to each receiver is approximately the same $\theta_1 \approx \theta_2 \approx \theta$.

We can express the time domain correlation of the signal in the frequency domain by using the generic Parseval's theorem. Knowing that the cross power spectral density for a stochastic stationary process is the Fourier transform of the time domain cross correlation function $(see\ appendix\ 1)$:

$$R_{x_{r,1}\,x_{r,2}}(0) = \int_{-\infty}^{\infty} \frac{\overline{X_1(\bar{r}_i, f) X_2^*(\bar{r}_i, f)}}{4\, R_a}\, H_{r,1}(f) H_{r,2}^*(f)\, df \tag{4.13}$$

The term $\frac{\overline{X_1(\bar{r}_i,f)X_2^*(\bar{r}_i,f)}}{4R_a}$ is the cross power spectral density of the extended source. It is the sum of the spectral brightness of all the points i of the source coming to both antennas with a phase difference between them of $\frac{2\pi f \Delta r_i}{c}$ and is pondered by the response of the antenna in each direction with the corresponding effective length [8]:

$$\frac{\overline{X_1(\bar{r}_i,f)X_2^*(\bar{r}_i f)}}{4R_a} = \frac{K_B}{\sqrt{\Omega_{r,1}\Omega_{r,2}}} \iint_{Source} T_B(\theta,\phi) F_{r,1}(\theta,\phi) F_{r,2}^*(\theta,\phi) e^{\frac{j2\pi f \Delta r_i}{c}} d\Omega \tag{4.14}$$

Taking into account (4.14) we have that the cross correlation function is :

$$R_{x_{r,1}\,x_{r,2}}(0) = \frac{K_B}{\sqrt{\Omega_{r,1}\Omega_{r,2}}} \int_{-\infty}^{+\infty} \iint_{Source} T_B(\theta,\phi) F_{r,1}(\theta,\phi) F_{r,2}^*(\theta,\phi)\; H_{r,1}(f) H_{r,2}^*(f) e^{\frac{j2\pi f \Delta r_i}{c}} df\, d\Omega \tag{4.15}$$

The frequency integral is where the fringe washing function appears and is the term that takes into account the decorrelation effects due to the different arrival times of the target's signal to each antennas and the bandwidth of the filters when correlating:

$$\int_{-\infty}^{\infty} H_{r,1}(f)H_{r,2}^{*}(f)\, e^{\frac{j2\pi f\Delta r_i}{c}} df = B\sqrt{G_{r,1}}\sqrt{G_{r,2}}\; sinc_N\left(B\frac{\Delta r_i}{c}\right) e^{\frac{j2\pi f_0\Delta r_i}{c}} \qquad (4.16)$$

Where $H_{r,1}(f) = \sqrt{G_{r,1}}\;\prod(\frac{f-f_0}{B}+\frac{B+1}{2})$, $H_{r,2}(f) = \sqrt{G_{r,2}}\;\prod(\frac{f-f_0}{B}+\frac{B+1}{2})$ are filters that centers $x_1(t)$ and $x_2(t)$ to f_0 with bandwidth B and receiver gains $\sqrt{G_{r,1}}$, $\sqrt{G_{r,2}}$.

For ideal squared transfer function filters, the fringe washing function is defined as the normalized sinc function:

$$\tilde{r}(t) = sinc_N(B\,t) \qquad (4.17)$$

In our case the $\tilde{r}\left(\frac{\Delta r_i}{c}\right)$ term limits the bandwidth of our signal reducing the sensitivity of the system. Note that $\frac{\Delta r_i}{c} \ll \frac{1}{B}$ in order to avoid decorrelation effects, that is in other words reducing the field of view of the system, the maximum baseline separation or the bandwidth of the system.

And the general expression of the cross correlation in terms of the fringe washing function is :

$$R_{x_{r,1}\,x_{r,2}}(0) = \frac{K_B B\sqrt{G_{r,1}G_{r,2}}}{\sqrt{\Omega_{r,1}\Omega_{r,2}}}\iint_{Source} T_B(\theta,\phi)F_{r,1}(\theta,\phi)F_{r,2}^{*}(\theta,\phi)\,\tilde{r}\left(\frac{\Delta r_i}{c}\right)e^{j2\pi f_0\frac{\Delta r_i}{c}}d\Omega \qquad (4.18)$$

It is convenient to express the coordinate system from the expression above in director cosines so it can be seen directly that the spatial Fourier transform of the modified brightness temperature is the cross correlation in the spatial frequency domain.

At large distances $R \gg d_1$, see Figure 4.3, we have that the distance from the source point to the antennas are:

$$r_{1i} \approx R + \frac{d_1^2}{2R} - (\frac{x_i}{R}x_1 + \frac{y_i}{R}y_1 + \frac{z_i}{R}z_1) \qquad (4.19)$$

$$r_{2i} \approx R + \frac{d_2^2}{2R} - (\frac{x_i}{R}x_2 + \frac{y_i}{R}y_2 + \frac{z_i}{R}z_2) \qquad (4.20)$$

Where (x_1, y_1, z_1), (x_2, y_2, z_2) are the cartesian coordinates of the antenna 1 and 2, and (x_i, y_i, z_i) are the coordinates of the source i.

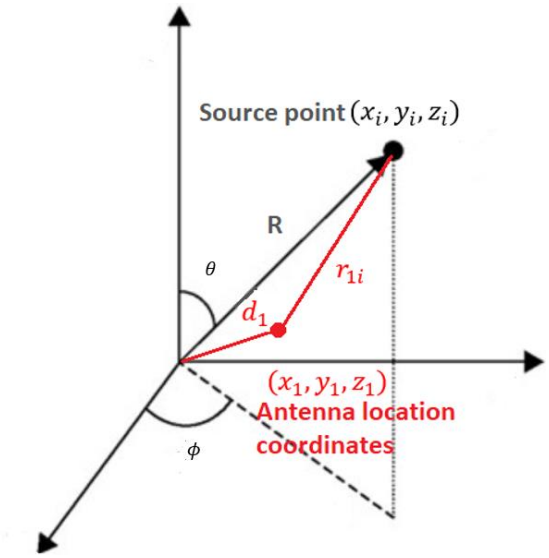

Figure 4.3 Cartesian coordinates illustrating the source point position, distance to origin of coordinates R, distance to the antenna 1, antenna's position and its distance to the origin.

To simplify the notation we can rewrite the expressions using director cosines :

$$\xi_i = \frac{x_i}{R} = sin(\theta)\, cos(\phi) \tag{4.21}$$

$$\eta_i = \frac{y_i}{R} = sin(\theta)\, sin(\phi) \tag{4.22}$$

Then for 2 close antennas in the x-y plane :

$$\Delta r_i = r_{2i} - r_{1i} \approx -\left[\xi_i(x_2 - x_1) + \eta_i(y_2 - y_1)\right] \tag{4.23}$$

The phase difference is $-k(r_{1i} - r_{2i}) \approx -2\pi(\xi_i u + \eta_i v)$ (4.24)

Where $u = \frac{x_2 - x_1}{\lambda_0}$ and $v = \frac{y_2 - y_1}{\lambda_0}$ are the normalized antenna spacing.

Then the cross correlation of the 2 received signals becomes:

$$R_{x_{r,1}\, x_{r,2}}(0) = \frac{K_B B \sqrt{G_{r,1} G_{r,2}}}{\sqrt{\Omega_{r,1}\Omega_{r,2}}} \iint\limits_{\eta^2+\xi^2 \le 1} \frac{T_B(\xi,\eta) - T_r}{\sqrt{1-\eta^2-\xi^2}} F_{r,1}(\xi,\eta) F_{r,2}^*(\xi,\eta) \tilde{r}\left(-\frac{u\xi + v\eta}{f_0}\right) e^{-j2\pi(u\xi+v\eta)} d\eta d\xi \tag{4.25}$$

$$with \quad d\Omega = \sin(\theta)\, d\theta d\phi = \frac{d\eta d\xi}{\sqrt{1-\xi^2-\eta^2}}$$

The term T_r is the equivalent temperature of the noise produced by the receivers and entering the antennas [8]. This noise is coupled from one antenna to the other. If receivers have input isolators, T_r is simply their physical temperature. Following from

(4.25) the visibility function is defined as for any pair of antennas (called baselines) k, j $(k \neq j)$:

$$V_{kj}(u_{kj}, v_{kj}) = \frac{1}{\sqrt{\Omega_{r,1}\Omega_{r,2}}} \iint_{\eta^2+\xi^2\leq 1} \frac{T_B(\xi,\eta) - T_r}{\sqrt{1-\eta^2-\xi^2}} F_{r,1}(\xi,\eta) F^*_{r,2}(\xi,\eta) sinc_N\left(-B\frac{u_{kj}\xi + v_{kj}\eta}{f_0}\right) e^{-j2\pi(u_{kj}\xi+v_{kj}\eta)} d\eta d\xi \tag{4.26}$$

With (4.26) and (4.27) we can see that the visibility function is the cross correlation divided by $K_B B\sqrt{G_{r,k}G_{r,j}}$ for any pair of antennas :

$$V_{kj}(u_{kj}, v_{kj}) = \frac{R_{x_{r,}\, x_{r,j}}(0)}{K_B B\sqrt{G_{r,k}G_{r,j}}} \tag{4.27}$$

In Figure 4.4 we can see a T-shape SAR covering two dimensions, horizontal for u and vertical for v. All the baselines in the same x for example with the same length are redundant, the same as for the y axis so if receivers are identical their cross correlation are the same hence the visibility is the same.

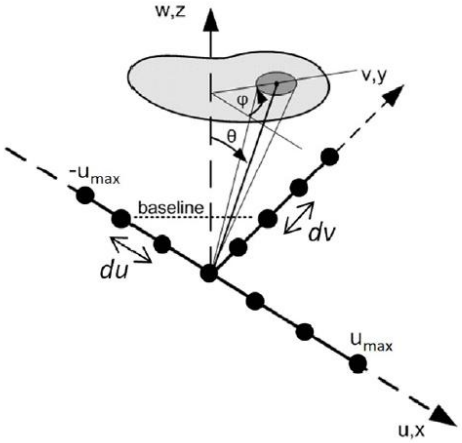

Figure 4.4 Geometry of a T-shape antenna pattern for a synthetic aperture interferometric radiometer from [6].

If we define $T'_B(\xi,\eta) = \frac{T_B(\xi,\eta)-T_r}{\sqrt{\Omega_{r,1}\Omega_{r,2}}\sqrt{1-\eta^2-\xi^2}} F_{r,1}(\xi,\eta) F^*_{r,2}(\xi,\eta) sinc_N\left(-B\frac{u_{kj}\xi+v_{kj}\eta}{f_0}\right)$ as the modified brightness temperature of the scene including the antenna patterns, the fringe washing function and the T_r term, we may arrive to :

$$V_{kj}(u_{kj}, v_{kj}) = \iint_{\eta^2+\xi^2\leq 1} T'_B(\xi,\eta)\, e^{-j2\pi(u_{kj}\xi+v_{kj}\eta)} d\eta d\xi \tag{4.28}$$

The visibility is the Fourier transform of the modified brightness temperature :

$$V_{kj}(u_{kj}, v_{kj}) = \frac{R_{x_{r,}\, x_{r,j}}(0)}{K_B B\sqrt{G_{r,k}G_{r,j}}} = \mathcal{F}\left[T'_B(\xi,\eta)\right] \tag{4.29}$$

4.2.2 Image Reconstruction & Field of view

According to the previous results, the reconstruction of the brightness temperature distribution from measurements of the visibility function can, in principle be carried out by an inverse Fourier transform.

$$T_B'(\xi,\eta) = \int_{-\infty}^{+\infty}\int_{-\infty}^{+\infty} V(u,v)\, e^{j2\pi(u\xi+v\eta)}\, du dv \tag{4.30}$$

Where it is implicitly assumed that visibility measurements are available at all possible spatial frequency components, u and v. In practice, visibility measurements correspond to discrete baseline separations between pairs of elements in the antenna array. The resulting truncated and discretized version of the image reconstruction algorithm follows as:

$$\widehat{T_B'}(\xi,\eta) = \sum_{k=-N}^{N}\sum_{j=-M}^{M} V(u_k,v_j) e^{j2\pi(u_k\xi+v_j\eta)} \tag{4.31}$$

The Field of View (FoV) of the system is limited by Nyquist sampling theorem, that is the shortest baseline as follows :

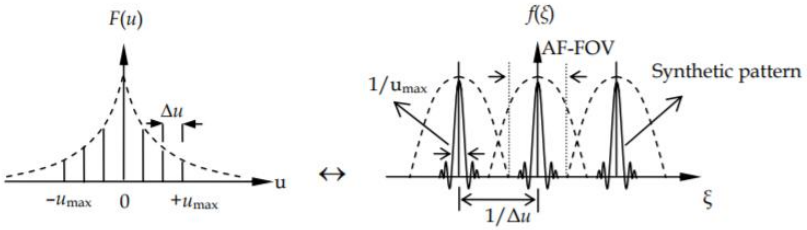

Figure 4.5 Nyquist Sampling theorem

$$\text{That is :} \quad \Delta u < \frac{1}{2\xi_{max}} \text{ and } \Delta v < \frac{1}{2\eta_{max}} \tag{4.32}$$

If the minimum separation are longer than the constrained ones in (4.32), we will have aliasing effect.

4.2.3 Radiometric resolution

As the number of visibility samples are constrained by the total number of antennas, therefore the (u,v) domain is windowed with a window $W(u,v)$ that extends to the array size (u_{max}, v_{max})

$$T_B'(\xi,\eta) = \iint W(u,v)V(u,v)\, e^{j2\pi(u\xi+v\eta)}\, du dv \tag{4.33}$$

The integral is the inverse Fourier transform of $W(u,v)\cdot V(u,v)$, which is equivalent as the convolution of the inverse Fourier transform of W and V :

$$T_B'(\xi,\eta) = \iint T_B'(\xi',\eta')\, AF(\xi-\xi',\eta-\eta')d\xi' d\eta' \tag{4.34}$$

Where the inverse Fourier transform of W is the antenna array factor AF [3]:

$$AF(\xi,\eta) = sinc(2u_{max}\xi)sinc(2v_{max}\eta) \tag{4.35}$$

Equation (4.35) is essentially a spatial low-pass filter of the equivalent brightness temperature distribution. The resolution of the reconstructed image can be defined as the angular distance between the half power of the AF for both x and y axes :

$$\Delta\theta_x \cong \Delta\xi = \frac{0.60}{u_{max}} = \frac{0.60}{\Delta x_{max}}\lambda \tag{4.36}$$

$$\Delta\theta_y \cong \Delta\eta = \frac{0.60}{v_{max}} = \frac{0.60}{\Delta y_{max}}\lambda \tag{4.37}$$

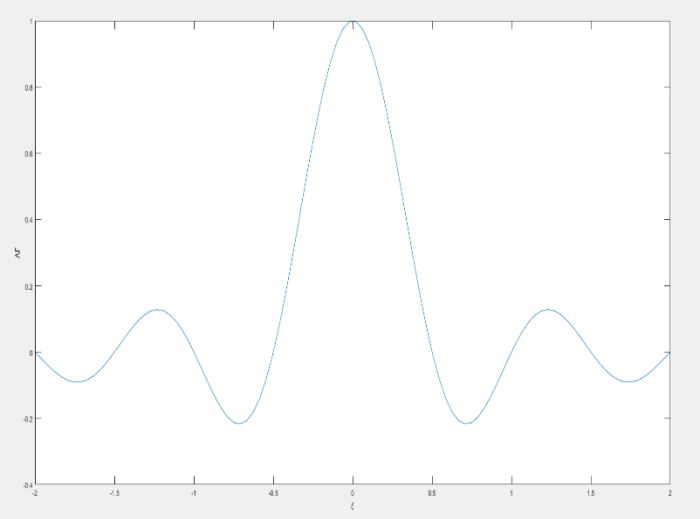

Figure 4.6 Array Factor for $u_{max} = 1$ and ξ ranging from $-\frac{2}{u_{max}}$, $\frac{2}{u_{max}}$.

So in order to achieve high angular resolution, we need either high frequencies or longer maximum baseline u_{max}.

4.2.4 SA Radiometric sensitivity

The sensitivity of the visibility samples of the SAR ΔT_v equals the sensitivity of the TPR [7]:

$$\Delta T_v = \frac{T_{ph} + T_{REC}}{\sqrt{B\tau}} \tag{4.38}$$

The radiometric sensitivity of the real brightness temperature of a SAR taking into account the image reconstruction algorithm, and the whole receiver parameters was carried out by the research group of remote sensing from UPC in 1998 [9]:

$$\Delta T_B(\xi,\eta) = \Delta S \frac{T_{ph}+T_{REC}}{\sqrt{B\tau}} \frac{\sqrt{\Omega_{r,1}\Omega_{r,2}}}{F_{r,1}(\xi,\eta)F^*_{r,2}(\xi,\eta)} \sqrt{1-\xi^2-\eta^2}\, \frac{\alpha_w \alpha_s}{\alpha_f} \sqrt{N_v} \tag{4.39}$$

Where ΔS is the elementary area in (ξ,η), α_w is a parameter that depends on the window, α_s takes into account the sensitivity loss due to non-analog correlation, α_f takes into account the pre-detection filter shape and N_v is the total number of visibility samples.

4.3 CONCLUSIONS OF THIS CHAPTER

SUMMARY

Decorrelation effect : Fringe washing function

$$sinc_N\left(B\frac{\Delta r}{c}\right)$$

Sensitivity of the SAR:

$$\Delta T_B \propto \frac{T_{ph}+T_{REC}}{\sqrt{B\tau}} \sqrt{N_v}$$

with τ =integration time and $N_v$number of visibility samples

Angular resolution :

$$\Delta\theta_x \cong \Delta\xi = \frac{0.60}{u_{max}} = \frac{0.60}{\Delta x_{max}}\lambda$$

Δx_{max}=maximum baselines separation

The study throughout this chapter has provided insight into the inherent trade-offs in the design of a SA radiometer, which may be summarized as follows.

- Field of View, bandwidth, fringe washing function decorrelation effects, Radiometer accuracy, radiometer sensitivity are all related.

- For high sensitivity we need high Bandwidth, but the decorrelation effect is going to get bigger and one possible solution is reducing the field of view.

- For high angular accuracy we need to work in higher frequencybands, or longer baselines, but if we use longer baselines, we get more decorrelation as sources will come with bigger $\frac{\Delta r}{c}$ and can't use very high bandwidth.

- Integration time is something to take it into account too as it reduces the standard deviation so increases radiometer sensitivity.

In the next chapters we are going to apply these concepts and relationships to assess the advantages and challenges related to the introduction of photonic components in a microwave band SA radiometer.

5. Phase modulator PM

The LiNbO3 optical phase modulator is based on a LiNbO3 crystal where the signal travels through. The phase of the signal is controlled by a voltage V between the electrodes as :

$$\Delta\phi = \frac{\pi n_0^3 r V}{\lambda_0}\frac{l}{d} = \frac{\pi}{V_\pi}V \tag{5.1}$$

where d is the electrode separation, r is an electro-optic coefficient that depends on the polarization of the optical and electric beams, $n_0$is the LiNbO3 index of refraction, l is the length of the interaction between the electrical and the optical signals and λ_0 is the optical wavelength. V_π is a characteristic modulator voltage defined as the voltage required for a π phase shift of the optical wave by the electrooptical effect.

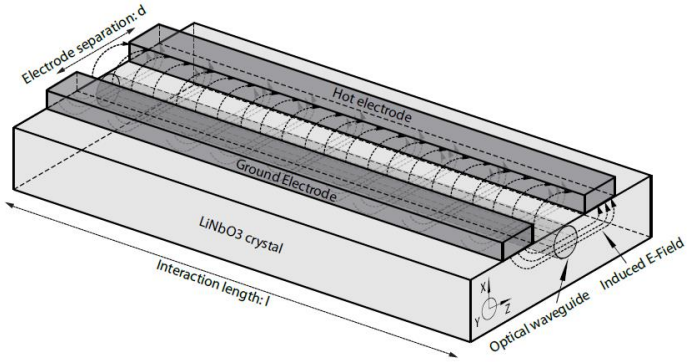

Figure 5.1 shows a schematic of a LiNbO3 phase modulator where the electrodes, the optical waveguide and the direction of the electric field are depicted.

LiNbO3 crystals are birefringent and thus their refractive and nonlinear indices depend on the polarization of the optical wave. A consequence is that the modulation efficiency depends on the polarization of the optical and electrical waves. Commercial modulators usually incorporate a polarization maintaining fiber at their input with ensures that the input optical wave is polarized along the direction of maximum efficiency. In order to connect to standard fiber where the fundamental mode may be linearly polarized along any radial direction in a transversal plane, polarization controls are needed to avoid excessive insertion loss.

The output of a PM is the input laser source $E_{in}(t) = E_0 e^{j(\omega_0 t+\theta_0)}$ modulated by a RF signal $V = V_{rf}\cos(\omega_{rf}t + \theta_1)$:

$$E_{outPM}(t) = E_0 e^{j(\omega_0 t+\theta_0)} e^{j\frac{\pi}{V_\pi}V_{rf}\cos(\omega_{rf}t+\theta_1)} \tag{5.2}$$

Where E_0, ω_0, θ_0 are the laser field amplitude, frequency and initial phase. $V_{rf}, \omega_{rf}, \theta_1$

are the RF voltage amplitude frequency, initial phase respectively and $\frac{\pi}{V_\pi} V_{rf} = m$ is the index of modulation.

Considering the Jacobi Anger expansion :

$$e^{j\, m\, cos(\theta)} = \sum_{n=-\infty}^{\infty} i^n\, J_n(m)\, e^{jn\theta} \text{ and that } J_{-n}(m) = (-1)^n J_n(m)$$

$$E_{outPM}(t) = E_{in}(t)\big(J_0(m) + 2\sum_{n=1}^{\infty} i^n J_n(m) \cos\big(n\,(\omega_{rf} t + \theta_1)\big)\big) \tag{5.3}$$

Expanding the Bessel functions just until second order n=2, because higher orders are relatively negligible with respect to the first 2 orders if $m \ll 1$:

$$E_{outPM}(t) = E_{in}(t)\Big(\,\beta_0 + j2\beta_1 \cos\big(\omega_{rf} t + \theta_1\big) - 2\beta_2 \cos\Big(2\big(\omega_{rf} t + \theta_1\big)\Big)\Big) \tag{5.4}$$

Where it's been defined that :

$$\beta_0 = J_0(m)\ ;\ \beta_1 = J_1(m) \approx \frac{m}{2}\ ;\ \beta_2 = J_2(m) \tag{5.5}$$

Which is the same as expanding the exponential form with a Taylor expansion until second order :

$$e^{jm\cos(\omega_{rf} t + \theta_1)} \approx 1 + jm\cos(\omega_{rf} t + \theta_1) - \frac{1}{2} m^2 \cos^2(\omega_{rf} t + \theta_1) =$$
$$1 - \tfrac{m^2}{4} + jm\cos(\omega_{rf} t + \theta_1) - \tfrac{m^2}{4}\cos(2(\omega_{rf} t + \theta_1)) \tag{5.6}$$

By equivalency of (5.4) and (5.6) we have that :

$$\beta_0 \approx 1 - \beta_1^2$$
$$\beta_1 = \beta_1$$
$$\beta_2 \approx \tfrac{1}{2}\beta_1^2$$

We can express all the terms as a function of β_1

$$e^{j\frac{\pi}{V_\pi} V_{rf}\cos(\omega_{rf} t + \theta_1)} \approx \big(1 - \beta_1^2\big) + 2j\beta_1\cos(\omega_{rf} t + \theta_1) - \beta_1^2\cos(2(\omega_{rf} t + \theta_1)) \tag{5.7}$$

6. Photonic correlators

In this chapter, the most basic photonic correlator is presented. The main problem of this kind of correlators is shown and ongoing works trying to solve this problem are then presented.

6.1 Basic photonic correlator

Figure 6.1 shows the scheme of a basic correlator formed by 2 antennas, a filter that centers our RF signal to f_m with bandwidth B as in Figure 4.2 but now the RF signals $x_{r,i}(t) = Re(\, n_i(t)\, e^{j\omega_m t}\,)$ are upconverted to the optical domain by modulating the laser source 1. After that, they are coupled, filtered and photo detected. As we are going to see later, in this last element is where the correlation is done.

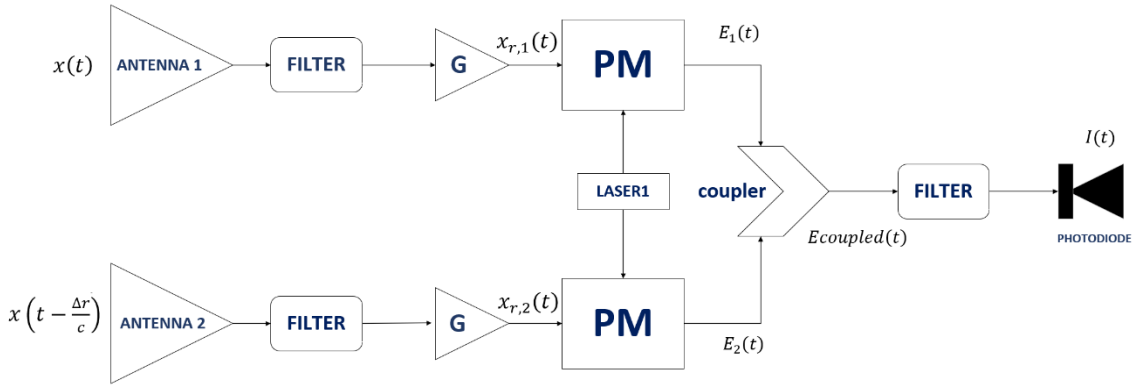

Figure 6.1 Scheme of a basic photonic correlator

The modulated signal at the output of each PM using (5.6) is:

$$E_1(t) = \frac{E_0}{\sqrt{2}}\, e^{j(\omega_0 t+\theta_1)} e^{j\alpha_1} \left(1 + j\frac{\pi\, x_{r,1}(t)}{V_\pi} - \frac{1}{2}\left(\frac{\pi\, x_{r,1}(t)}{V_\pi}\right)^2 + O^3\right) + E_{noise1} \tag{6.1}$$

$$E_2(t) = \frac{E_0}{\sqrt{2}} e^{j(\omega_0 t+\theta_1)} e^{j\alpha_2} \left(1 + j\frac{\pi\, x_{r,2}(t)}{V_\pi} - \frac{1}{2}\left(\frac{\pi\, x_{r,2}(t)}{V_\pi}\right)^2 + O^3\right) + E_{noise2} \tag{6.2}$$

Where E_{noise1} and E_{noise2} are the errors due to receiver chain 1 and 2, for example baseline positions, antenna's errors… In order to simplify notations we can suppose that they are negligible, but they should be taken into account in further studies. α_1 and α_2 are the phase errors introduced by fiber vibrations, little temperature variations etc… We can suppose that they can go from 0 to 2π randomly.

$E_1(t)$ and $E_2(t)$ are coupled and supposing identical receivers, that is $x_{r,2}(t) = x_{r,1}\left(t - \frac{\Delta r_i}{c}\right)$ we have :

$$E_{coupled}(t) = \frac{E_0}{\sqrt{2}} e^{j\alpha_1} e^{j(\omega_0 t+\theta_1)} \left(\left(1 + j\frac{\pi\, x_{r,1}(t)}{V_\pi} - \frac{1}{2}\left(\frac{\pi\, x_{r,1}(t)}{V_\pi}\right)^2\right) + e^{j\alpha}\left(1 + j\frac{\pi\, x_{r,1}\left(t-\frac{\Delta r_i}{c}\right)}{V_\pi} - \frac{1}{2}\left(\frac{\pi\, x_{r,1}\left(t-\frac{\Delta r_i}{c}\right)}{V_\pi}\right)^2\right)\right) \quad (6.3)$$

Where $\alpha = \alpha_2 - \alpha_1$ is the relative phase error.

Given that $x_{r,i}(t)$ is a passband signal with center frequency f_m, $E_{coupled}(t)$ will be mainly composed of five basic spectral terms: one at the optical carrier frequency f_0 and two sidebands at each side of the optical carrier, at f_0+f_m, f_0-f_m, f_0+2f_m and f_0-2f_m.

We will refer the spectral components f_0+f_m and f_0+2f_m as upper sidebands (USBs), $f_0 - f_m$ and $f_0 - 2f_m$ as lower sidebands (LSBs).

If we filter the carrier and the USBs and using for $x_{r,i}(t)$ the expression in terms of the phase quadrature baseband signals $x_{r,i}(t) = n_{Ii}(t)\cos(\omega_m t) - n_{Qi}(t)\sin(\omega_m t)$ we get:

$$E_{filtered}(t) = \frac{E_0}{\sqrt{2}}\, e^{j\alpha_1} e^{j(\omega_0 t+\theta_1)} \left(1 - \left(\frac{\pi}{2V_\pi}\right)^2 \|n_1(t)\|^2 + j\frac{\pi}{2V_\pi} n_1(t) e^{j\omega_m t} - \left(\frac{\pi}{2V_\pi}\right)^2 n_1^2(t) e^{j2\omega_m t} + e^{j\alpha}\left(1 - \left(\frac{\pi}{2V_\pi}\right)^2 \left\|n_1\left(t-\frac{\Delta r_i}{c}\right)\right\|^2 + j\frac{\pi}{2V_\pi} n_1\left(t - \frac{\Delta r_i}{c}\right) e^{j\omega_m\left(t-\frac{\Delta r_i}{c}\right)} - \left(\frac{\pi}{2V_\pi}\right)^2 n_1^2\left(t-\frac{\Delta r_i}{c}\right) e^{j2\omega_m t}\right)\right) \quad (6.4)$$

Photodetecting the filtered signal , the instant photocurrent is by the square rule of the photodetector:

$$I(t) = \left\|E_{filtered}(t)\right\|^2 = \frac{E_0^2}{2}\left[\, 2 - \left(\frac{\pi}{2V_\pi}\right)^2 \left(\|n_1(t)\|^2 + \left\|n_1\left(t-\frac{\Delta r_i}{c}\right)\right\|^2\right) + 2\cos(\alpha)\left(1 - \left(\frac{\pi}{2V_\pi}\right)^2 \left(\|n_1(t)\|^2 + \left\|n_1\left(t-\frac{\Delta r_i}{c}\right)\right\|^2\right)\right) + \left(\frac{\pi}{2V_\pi}\right)^2 2Re\left(n_1(t) n_1^*\left(t-\frac{\Delta r_i}{c}\right) e^{j\omega_m\frac{\Delta r_i}{c}} e^{-j\alpha}\right)\right] \quad (6.5)$$

The terms $\|n_1(t)\|^2$, $\left\|n_1\left(t-\frac{\Delta r_i}{c}\right)\right\|^2$ from (6.5) are the base band noise powers, and $n_1(t) n_1^*\left(t-\frac{\Delta r_i}{c}\right) e^{j\omega_m\frac{\Delta r_i}{c}} e^{-j\alpha}$ is the baseband cross terms multiplied by the phase error. Note that from the above is for a point source. If considering an incoherent extended source the average of the current $I(t)$ is, by superposition from each point *(see appendix 3):*

$$\overline{I(t)} = \frac{E_0^2}{2T}\int_0^T 2 - \left(\frac{\pi}{2V_\pi}\right)^2 \left(\overline{\|n_1(t)\|^2} + \overline{\left\|n_1\left(t-\frac{\Delta r_1}{c}\right)\right\|^2}\right) + 2\cos(\alpha)\left(1 - \left(\frac{\pi}{2V_\pi}\right)^2 \left(\overline{\|n_1(t)\|^2} + \overline{\left\|n_1\left(t-\frac{\Delta r_1}{c}\right)\right\|^2}\right)\right) + 2\left(\frac{\pi}{2V_\pi}\right)^2 Re\left(\overline{n_1(t) n_1^*\left(t-\frac{\Delta r_1}{c}\right) e^{j\omega_m\frac{\Delta r_1}{c}} e^{-j\alpha}}\right) dt \quad (6.6)$$

Remember from section 4 that the bar " $\overline{\ }$ " notation denotes the contribution from all the points of the extended source.

The average of the baseband noise power is:

$$\frac{1}{T}\int_T \overline{\left\| n_1\left(t-\frac{\Delta r_i}{c}\right)\right\|^2}\,dt = \frac{1}{T}\int_T \overline{\|n_1(t)\|^2}\,dt = \iint_{source} \frac{k_B B G R_a}{\Omega} T_B(\theta,\varphi) t(\theta,\varphi)\,d\Omega = V_n^2 \tag{6.7}$$

Note that $V_n^2 = P_a\, R_a$ being P_a from (3.22) the power captured by one of the antennas from the extended source.

The average of the cross terms is the cross correlation of the baseband signals $n_1(t)$ and $n_2(t)$. It is the same as the cross correlation of $x_{r,1}(t)$ and $x_{r,2}(t)$ from (4.27) but assuming identical receivers and no normalized voltages (*see appendix 4*), therefore:

$$\frac{1}{T}\int_0^T \overline{n_1(t) n_1^*\left(t-\frac{\Delta r_i}{c}\right) e^{J\omega_m \frac{\Delta r_i}{c}}} = R_{n_1\, n_2}(0) = R_{x_{r,1}\, x_{r,2}}(0) = V_{12} K_B B\, R_a G \tag{6.8}$$

Then the equation from (6.6), taking into account (6.7) and (6.8) :

$$\overline{I(t)} = E_0^2\left(2 + 2\cos(\alpha) - 2\left(\frac{\pi}{2V_\pi}\right)^2 V_n^2(1+2\cos(\alpha)) + \left(\frac{\pi}{2V_\pi}\right)^2 2 * Re(V_{12} K_B B R_a G e^{-j\alpha})\right) \tag{6.9}$$

In order to isolate the visibility from the measurement of $\overline{I(t)}$ we need to know V_n^2 and α. V_n^2 can be measured if we filter the carrier and upper sidebands of $E_1(t)$ before combining with $E_2(t)$, and averaging the photodetected current.

However α is a randomly fast changing value during our integration time this phase error may have changed. If we do not control it fast enough, the correlator is unfeasible.

We also need both the real part and the imaginary part of the visibility separately so we can inverse Fourier transform without ambiguity. In the next section we are going to see recent works that will try to compensate for this phase error α .

6.2 Ongoing work

Nova in his Doctoral thesis in 2015 [7] worked on the advantages of photonics in signal distribution by using waveguides to couple the signals from different baselines in order to avoid the random phase error, that is in other words setting $\alpha = 0$ physically.

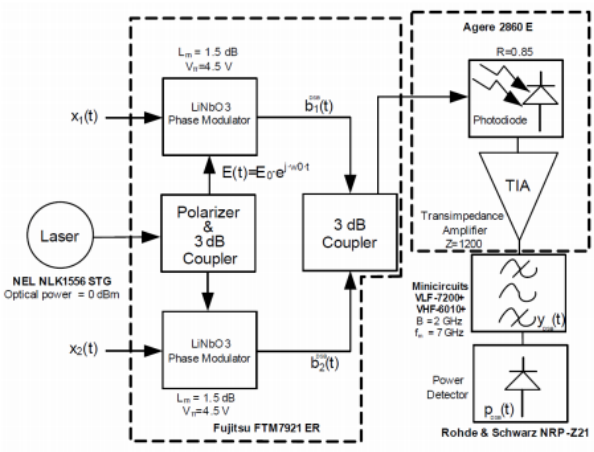

Figure 6.2 Schematic of optical modulation and combination in the left hand side followed by a microwave correlation in the right hand side. The dashes lines represents a compact device.

This scheme follows the same basic structure as that in Figure 6.1 but, using a bandpass electrical filter after coupling and photodetecting . Finally an electrical power detector carries out the correlations and the image is reconstructed by software. However, as $\alpha = 0$ just the real part of the correlation will be detected, also the power from the extended source P_n is not measured and masks the visibilities. A phase switching technique is proposed in [6] to solve these 2 problems, by adding a phase shift of π and $\pi/2$ alternatively to one of the RF signals, the real part and imaginary part of the visibility may be obtained, at the cost of reducing the integration time by a factor 2.

In addition, in [6] a free-space combination scheme for an arbitrary number of front-end receivers is proposed, as depicted in Figure 6.3. The combination can be performed in the free-space by using guiding optical beams with low divergence and with high spatial density.

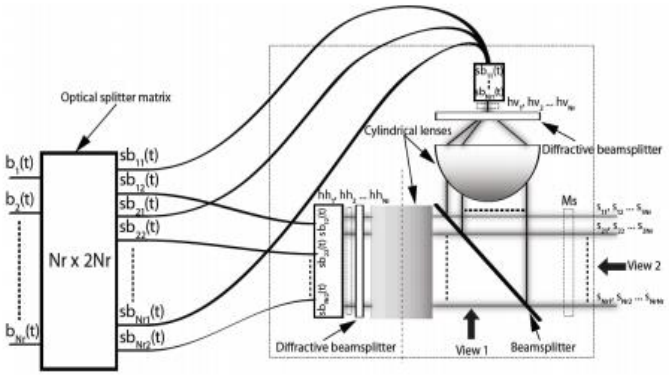

Figure 6.3 Scheme of the optical signals combination proposed in [6]

The first proposal of using photonics in order to obtain the correlations of each pair of receivers dates back to 1999 in a seminal paper by Blanchard [3], in which a technique called coherent optical beam forming is proposed. As illustrated in Figure 6.4, the principle of coherent optical beam forming is to first upconvert the RF signals collected by the antennas to optical frequency by means of EOMs, then transfer them with optical fibers and by using a lens, the Fourier transform and correlations are directly obtained in the ccd camera.

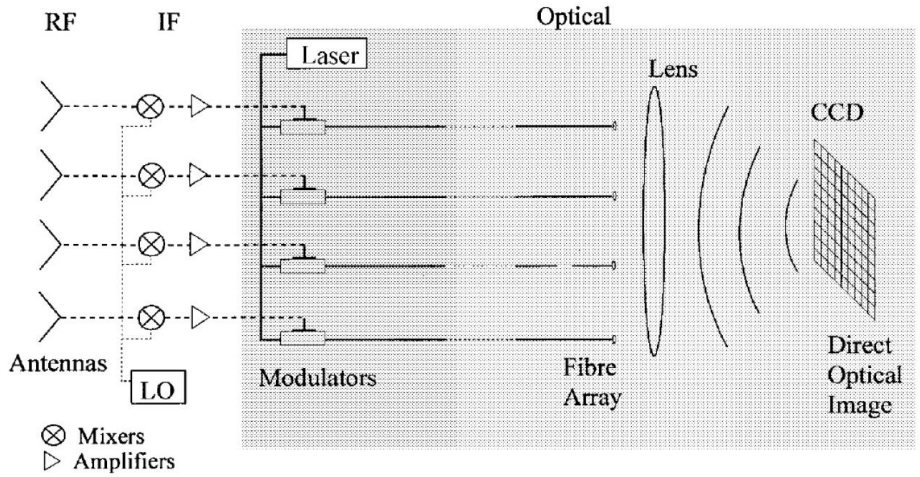

Figure 6.4 Coherent optical beam forming scheme proposed by Blanchard in 1999.

Since the image is formed through interference between the optical signals from each receiver, as we have seen before, phase control is critical. Blanchard proposes a technique called Redundant Spacings Calibration (RSC) [10] .

This technique is based on using the redundancy of the baselines in order to extract the phase error, as the redundant baselines measure the same Fourier component of the source. If supposing two baselines, by measuring the image twice with a phase shift of π being added for the second measurement, the fringes are shifted by half a period $\cos(\theta) \rightarrow -\cos(\theta)$, hence if the two images are added together the fringes should cancel out. The fringes from the other baseline do not shift between the two images and hence add constructively, allowing the phase error of this baseline to be extracted without ambiguity. If the two images are then subtracted from each other, rather than added, the cancellation of fringes is reversed, and the phase error of the second baseline in the pair can be extracted. In order to measure the two images simultaneously, they have developed a technique using simple optics, a diffraction grating and a single CCD. This allows all of the baseline error phases to be extracted in a single snapshot, which is advantageous when phase errors are changing rapidly.

Once the phase error is extracted, each fiber contains a phase controller consisting of a piezoelectric drum which is used to correct the extracted phase error by applying a voltage controlled via PC (1 V gives π radians phase shift).

In 2014, a research group from Beihan university in China, based on the principal idea of Blanchard's approach applied a different phase calibration technique based on a

feedback loop [5]. It consists on a real-time phase controller that compares each optical beam of the fiber array to a reference one as shown in Fig. 6.5.

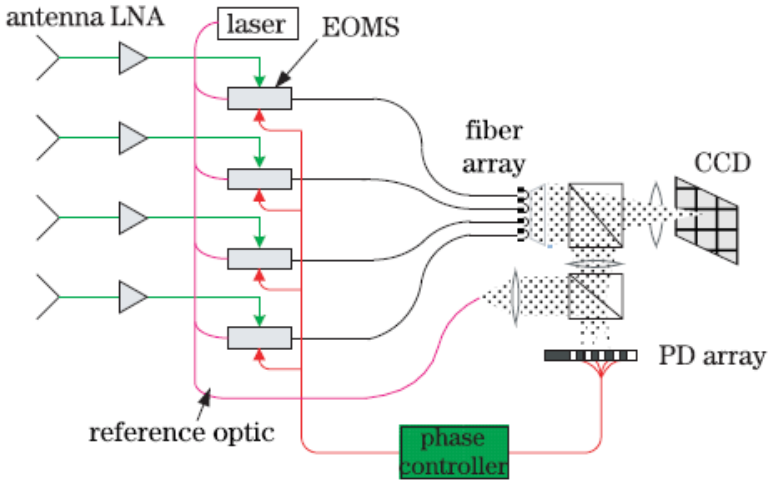

Figure 6.5 Scheme using active phase controller

The first order sidebands (FSBs) carry the amplitude and the phases of the incident signals from the source. The carrier is used to extract the phase error and is separated from the FSBs and higher order sidebands using a filter.

If supposing the carriers from two optical beams as :

$$E_{c1}(t) = A\, e^{j\alpha_1(t)} e^{j(\omega t+\theta_1)} \tag{6.10}$$

$$E_{c2}(t) = A\, e^{j\alpha_2(t)} e^{j(\omega t+\theta_1)} \tag{6.11}$$

Where A is the amplitude of the carrier, α_1 and α_2 the phase errors.

The interference between these two signals once photodetected can be expressed :

$$I_{ph}(t) = \|E_{c1}(t) + E_{c2}(t)\|^2 = 2A^2\left[1 + \cos\left(\alpha(t)\right)\right] \tag{6.12}$$

Where $\alpha(t) = \alpha_2(t) - \alpha_1(t)$.

So it is possible to calibrate the phase error using this intensity. They use a closed-loop control system for each baseline, the phase-modulated optical signal in the fiber array are collimated with the refractive lens array and passes through a 50/50 beam splitter.

One of the output beams passes through a filter to obtain the first order sidebands (FSB) for imaging, while the other with carrier beams is used for phase calibration as depicted in Figure 6.6. These carrier beams are overlapped by the reference light which passes through the beam expander and collimator. Then, the two kinds of beams will travel to

a micro lens array and be focused on the photonic detectors (PD). By the PD array, we can get voltages of the PD outputs which are individually proportional to the interference intensities between each carrier and the reference light. Thereafter, an algorithm based on stochastic parallel gradient descent (SPGD) [5], with these collected voltages it is thus able to correct the phase errors by controlling the Bias voltage of an electro optic modulator (EOM) .

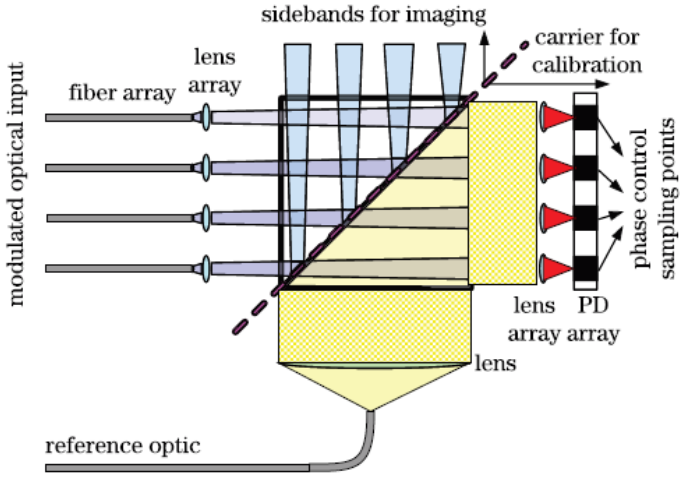

Figure 6.6 Optical configuration where carrier is for calibration and sidebands for imaging.

In order to compensate a phase error of 1Hz, it is proved that a feedback loop frequency of 1KHz is needed. However if phase errors $\Delta\alpha(t)$ are fast, of the order of 100Hz the system can't correct well even with a feedback frequency of 100KHz.

While Enrique avoids the phase errors by using waveguides , Blanchard and YuntaoHe used a feedback loop compensation with the drawback of how fast this phase error changes. We present a novel technique based on remodulating the signals which avoids both the feedback loop compensation and the waveguides, making the correlations in the optical domain by exploiting the advantadges of photonics As correlations are a DC value proportional to the sampled visibility function at the antenna pair positions, we highly reduce the complexity of electronic devices.

7. Our Proposal

In this last chapter, we will first present the design for a signal coming from an extended source, then we will particularize for a point source. Finally, simulation and experimental results are shown for a point source.

7.1 Photonic correlator based on Remodulation technique

Figure 7.1 shows the scheme of the remodulation technique. First of all, the signal from the first receiver $x_{r,1}(t)$ is going to modulate the laser 1 source at ω_1, the output of the first modulator is $E_{outPM1}(t)$ and is sent via fibers to the location of the second receiver, where it is coupled with the second laser at ω_2 and they are both modulated by $x_{r,2}(t+\tau)$, yielding $E_{outPM2}(t)$. The term $\tau = \frac{l_{fiber\ 1-2}}{c} n_{fiber}$ with $l_{fiber\ 1-2}$ the cable length in between antennas, c the velocity of light in vacuum and n_{fiber} the propagation index inside the fiber, is due to the fact that is $x_{r,1}(t)$ is delayed with a certain time $\tau = \frac{l_{fiber}}{c} n$ with respect to $x_{r,2}(t)$ caused by the mentioned fiber.

The laser source at ω_1 is modulated at PM1 (above in Figure 7.1) and then is remodulated at PM2 (below), while the laser source at ω_2 is modulated at PM2 only.

For a wide enough separation between ω_1 and ω_2, that is in our case 193.1THz and 193.2THz respectively, we can separate the modulated signal from the remodulated one with filter 1 and 2, which at the same time also filters out their LSBs. If we photodetect and then average the filtered remodulated signal $E_{rem\ 1}(t)$ we get a DC value proportional to the cross correlation and if we photodetect the filtered modulated signal $E_{mod\ 2}(t)$ we get a DC value proportional to the power of the signal so we can isolate the visibility function.

Filter 3 gets the entire modulated signal from receiver 2 so it can be used to continue remodulating with next antennas.

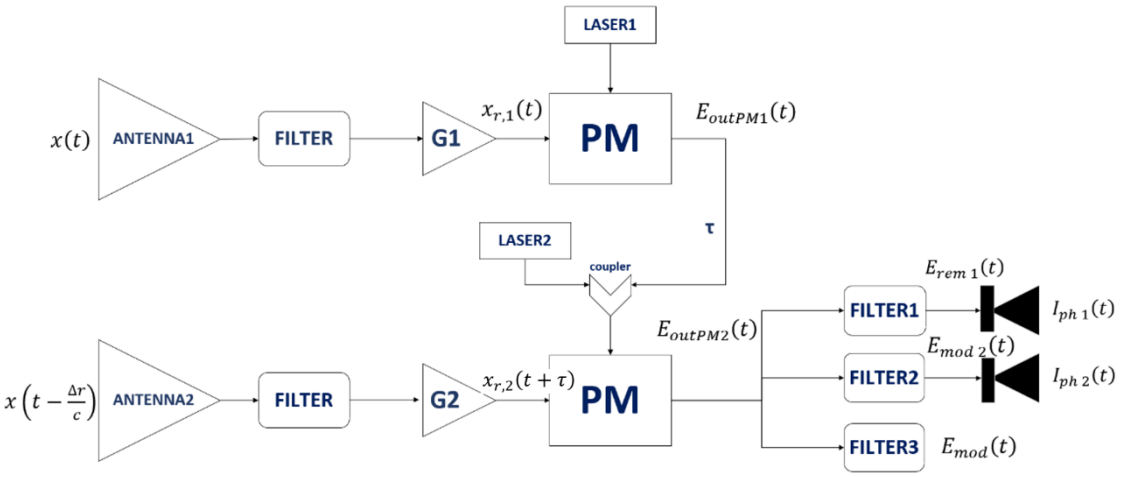

Figure 7.1 Scheme of remodulation technique

Next we proceed with the details of the setup step by step.

The output of the first PM from the first receiver is the laser 1 at ω_1, with an initial phase θ_1 modulated by the RF signal $x_{r,1}(t)$:

$$E_{outPM1}(t) = E_0 e^{j(\omega_1 t+\theta_1)} e^{j\frac{\pi x_{r,1}(t)}{V_\pi}} \tag{7.1}$$

$E_{outPM1}(t)$ is then sent via an optical fiber to the second receiver where it is coupled with the second laser at ω_2 and they are both modulated by $x_{r,2}(t+\tau)$, where τ takes into account the delay introduced by this last fiber. Both lasers will have a random phase α_1 *and* α_2 respectively at this point.

$$E_{outPM2}(t) = \left(E_0 e^{j(\omega_1 t+\theta_1)} e^{j\frac{\pi x_{r,1}(t)}{V_\pi}} e^{j\alpha_1} + E_0 e^{j(\omega_2(t+\tau)+\theta_2)} e^{j\alpha_2} \right) e^{j\frac{\pi x_{r,2}(t+\tau)}{V_\pi}} \tag{7.2}$$

It is seen in (7.2) that the laser source 1 at ω_1 is modulated by $x_{r,1}(t)$ and remodulated by $x_{r,2}(t+\tau)$ while the laser source 2 at ω_2 is just modulated by $x_{r,2}(t+\tau)$:

$$E_{remod}(t) = E_0 e^{j(\omega_1 t+\theta_1)} e^{j\frac{\pi x_{r,1}(t)}{V_\pi}} e^{j\alpha_1} e^{j\frac{\pi x_{r,2}(t+\tau)}{V_\pi}} \tag{7.3}$$

$$E_{mod}(t) = E_0 e^{j(\omega_2(t+\tau)+\theta_2)} e^{j\alpha_2} e^{j\frac{\pi x_{r,2}(t+\tau)}{V_\pi}} \tag{7.4}$$

Expanding (7.2) by Taylor until second order and supposing identical receivers in order to simplify notations, that is $x_{r,2}(t+\tau) = x_{r,1}\left(t - \frac{\Delta r_i}{c} + \tau\right)$ we get :

$$E_{outPM2}(t) = \left(E_0 e^{j(\omega_1 t+\theta_1)} e^{j\alpha_1} \left(1 + j\frac{\pi x_{r,1}(t)}{V_\pi} - \frac{1}{2}\left(\frac{\pi x_{r,1}(t)}{V_\pi}\right)^2 \right) + E_0 e^{j(\omega_2(t+\tau)+\theta_2+\alpha_2)} \right) \left(1 + j\frac{\pi x_{r,1}\left(t-\frac{\Delta r_i}{c}+\tau\right)}{V_\pi} - \frac{1}{2}\left(\frac{\pi x_{r,1}\left(t-\frac{\Delta r_i}{c}+\tau\right)}{V_\pi}\right)^2 \right) \tag{7.5}$$

The remodulated signal is separated from the modulated signal by filtering the carrier and USBs with filter 1 from the Figure 7.2 :

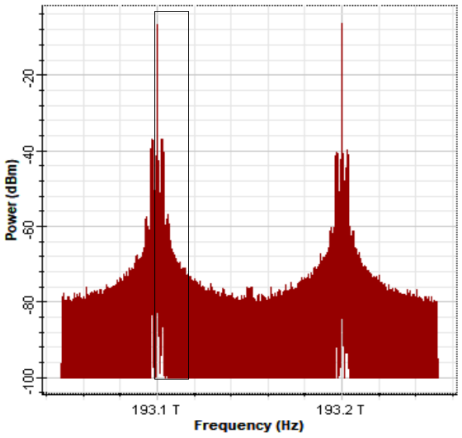

Figure 7.2 Spectral power density of $E_{outPM2}(t)$, we can see the remodulated signal at $\omega_1 = 193.1THz$ and the modulated signal at $\omega_2 = 193.2THz$. The rectangle simulates the ideal filter 1 that filters the carrier and upper sidebands of the remodulated signal.

The filtered remodulated signal is (see appendix 2):

$$E_{rem\,1}(t) = \frac{E_0}{\sqrt{3}} e^{j(\omega_1 t+\theta_1)} e^{j\alpha_1} \left(1 - 2\left(\frac{\pi}{2V_\pi}\right)^2 \left(n_1(t)^2 + n_1^2\left(t - \frac{\Delta r_i}{c} + \tau\right)\right) + j\,\frac{\pi\, n_1\left(t-\frac{\Delta r_i}{c}+\tau\right)}{2V_\pi} e^{j\omega_m\left(t-\frac{\Delta r_i}{c}+\tau\right)} + j\frac{\pi\, n_1(t)}{2V_\pi} e^{j\omega_m t} - 2\left(\frac{\pi}{2V_\pi}\right)^2 Re\left(n_1(t) n_1^*\left(t - \frac{\Delta r_i}{c} + \tau\right) e^{j\omega_m\left(\frac{\Delta r_i}{c}-\tau\right)}\right) + O^3 \right)$$

Assuming that the photodetector behaves as a low pass filter, terms at ω_m will not appear. The instantaneous photodetected current is :

$$I_{ph\,1}(t) = \frac{E_0^2}{3}\left(1 - \left(\frac{\pi}{2V_\pi}\right)^2 \left(|n_1(t)|^2 + \left| n_1\left(t - \frac{\Delta r_i}{c} + \tau\right)\right|^2\right) - 2\left(\frac{\pi}{2V_\pi}\right)^2 Re\left(n_1(t) n_1^*\left(t - \frac{\Delta r_i}{c} + \tau\right) e^{j\omega_m\left(\frac{\Delta r_i}{c}-\tau\right)}\right) + O^3\right) \qquad (7.7)$$

Averaging (7.7) and considering that we are receiving an incoherent extended source, as done in (6.6) and neglecting O^3 terms we have :

$$\overline{I_{ph\,1}(t)} = \frac{E_0^2}{3T}\int_T 1 - \left(\frac{\pi}{2V_\pi}\right)^2 \left(\overline{|n_1(t)|^2} + \overline{\left| n_1\left(t - \frac{\Delta r_i}{c} + \tau\right)\right|^2}\right) - 2\left(\frac{\pi}{2V_\pi}\right)^2 Re\left(\overline{n_1(t) n_1^*\left(t - \frac{\Delta r_i}{c} + \tau\right) e^{j\omega_m\left(\frac{\Delta r_i}{c}-\tau\right)}}\right) dt \qquad (7.8)$$

The average of the baseband instant noise powers $\overline{|n_1(t)|^2}$ and $\overline{\left| n_1\left(t - \frac{\Delta r_i}{c} + \tau\right)\right|^2}$ are $V_n^2 = \iint_{source} \frac{k_B B G R_a}{\Omega} T_B(\theta,\varphi) t(\theta,\varphi)\, d\Omega$.

The average of the cross terms is the cross correlation of the baseband signals $n_1(t)\ and\ n_2(t)$:

$$\frac{1}{T}\int_T \overline{n_1(t) n_1^*\left(t - \frac{\Delta r_i}{c} + \tau\right) e^{j\omega_m\left(\frac{\Delta r_i}{c}-\tau\right)}}\, dt = R_{n_1 n_2}(0) = k_B B G R_a V_{12} e^{-j\omega_m \tau} \qquad (7.9)$$

And the visibility of this baseline taking into account the time delay τ is :

$$V_{12} = \frac{1}{\Omega}\iint_{source} T_B(\theta,\varphi) t(\theta,\varphi) sinc_N\left(B\left(\frac{\Delta r_i}{c} - \tau\right)\right) e^{\,j\omega_m \frac{\Delta r_i}{c}} d\Omega \qquad (7.10)$$

For long baselines $x_{r,1}(t)$ will have to travel a distance at least equivalent to the length of this baseline in order to get remodulated by $x_{r,2}(t+\tau)$. This will increase τ and we are going to loose information as $sinc_N\left(B\left(\frac{\Delta r_i}{c} - \tau\right)\right) \to 0$, limiting the bandwidth, FoV and angular resolution. As correlations are available after τ, it also reduces our integration time. At the end of this chapter we will show a solution to that which is based on the synchronization of $x_{r,1}(t)$ and $x_{r,2}(t)$ so $\tau \approx 0$.

With (7.8) and (7.9), the averaged photo detected current neglecting higher order terms O^3 is:

$$\overline{I_{ph\,1}(t)} = \frac{1}{T}\int_T I_{ph\,1}(t)\,dt \approx \frac{E_0^2}{3}\left(1 - 2\left(\frac{\pi}{2V_\pi}\right)^2 V_n^2 - 2\left(\frac{\pi}{2V_\pi}\right)^2 Re\left(k_B BGR_a V_{12} e^{-j\omega_m \tau}\right)\right) \tag{7.11}$$

In order to measure V_n^2 we can filter with filter 2 the carrier and USBs of the modulated signal at ω_2 :

$$E_{mod\,2}(t) = \frac{E_0}{\sqrt{3}} e^{j(\omega_2(t+\tau)+\theta_2)} e^{j\alpha_2}\left(1 + j\frac{\pi}{2V_\pi} n_2(t+\tau) e^{jw_m(t+\tau)} - \left(\frac{\pi}{2V_\pi}\right)^2 \|n_2(t+\tau)\|^2 + O^3\right) \tag{7.12}$$

Photo detecting and averaging $E_{mod\,2}(t)$:

$$\overline{I_{ph\,2}(t)} = \frac{1}{T}\int_0^T |E_{mod\,2}(t)|^2\,dt \approx \frac{E_0^2}{3T}\int_0^T 1 - \left(\frac{\pi}{2V_\pi}\right)^2 \|n_2(t+\tau)\|^2\,dt = \frac{E_0^2}{3}\left(1 - \left(\frac{\pi}{2V_\pi}\right)^2 V_n^2\right) \tag{7.13}$$

The final expression of the visibility function multiplied by the delay term becomes :

$$\frac{\left(6\,\frac{\overline{I_{ph\,2}(t)}}{E_0^2} - 1 - \frac{\overline{I_{ph\,1}(t)}}{E_0^2}\right)}{2\left(\frac{\pi}{2V_\pi}\right)^2 R_a BGk_B} = Re\left(V_{12}\cdot e^{-j\omega_m\tau}\right) \tag{7.14}$$

As long as $e^{-j\omega_m\tau} = \pm j$ we detect the imaginary part of the visibility, and if $e^{-j\omega_m\tau} = \pm 1$ we get the real part. The only thing we need to do is to choose the right fiber length as $\tau = \frac{l_{fiber\,1-2}}{c} n_{fiber}$.

If we suppose detecting a point source (7.10) becomes:

$$V_{12} \approx T_B(\theta_0,\varphi_0)\,\frac{\iint_{point} t(\theta,\varphi)\,d\Omega}{\Omega}\,sinc_N\left(B\left(\frac{\Delta r_i}{c} - \tau\right)\right) e^{j\omega_m\left(\frac{\Delta r_i}{c} - \tau\right)} \tag{7.15}$$

Then the average at the photodiode 1 is :

$$\overline{I_{ph\,1}(t)} \approx E_0^2\left(1 - 2\left(\frac{\pi}{2V_\pi}\right)^2 V_n^2 - 2\left(\frac{\pi}{2V_\pi}\right)^2 V_n^2\,Re\left(sinc_N\left(B\left(\frac{\Delta r_i}{c} - \tau\right)\right) e^{j\omega_m\left(\frac{\Delta r_i}{c} - \tau\right)}\right)\right) \tag{7.16}$$

So the normalized visibility function is $C = V_{12} / \frac{T_B(\theta_0,\varphi_0)\iint_{point} t(\theta,\varphi)d\Omega}{\Omega}$:

$$C = \frac{\left(6\,\overline{I_{ph\,2}(t)} - E_0^2 - \overline{I_{ph\,1}(t)}\right)}{2\left(E_0^2 - \overline{I_{ph\,2}(t)}\right)} = sinc_N\left(B\left(\frac{\Delta r_i}{c} - \tau\right)\right)\cos\left(\omega_m\left(\frac{\Delta r_i}{c} - \tau\right)\right) \tag{7.17}$$

Where now $V_n^2 = R_a BGk_B \frac{T_B(\theta_0,\varphi_0)\iint_{point} t(\theta,\varphi)d\Omega}{\Omega}$ $[V^2]$

The real part of the normalized visibility function is

$$C = \pm sinc_N\left(B\left(\frac{\Delta r_i}{c} - \tau_r\right)\right)\cos\left(\omega_m \frac{\Delta r_i}{c}\right) \tag{7.18}$$

And the imaginary part is

$$C = \pm sinc_N\left(B\left(\frac{\Delta r_i}{c} - \tau_i\right)\right)\sin\left(\omega_m \frac{\Delta r_i}{c}\right) \tag{7.19}$$

Where the sign $\pm$ depends on the choice of $\tau\ \omega_m$.

Simulations and experimental lab are based on calculating this C term. The real part of the visibility for a point source is proportional to a cosine while the imaginary part to a sine and it will depend on the delay parameter τ introduced by the fiber as discussed previously.

We have only one possible choice of τ in this setup, so we will either detect only the real part or the imaginary part. A possible solution is to use the modulated signal from the second receiver after the filter 3 from figure 7.1 in order to remodulate it in the first PM too, so we have 2 correlations using 2 $\tau's$. See figure 7.3 :

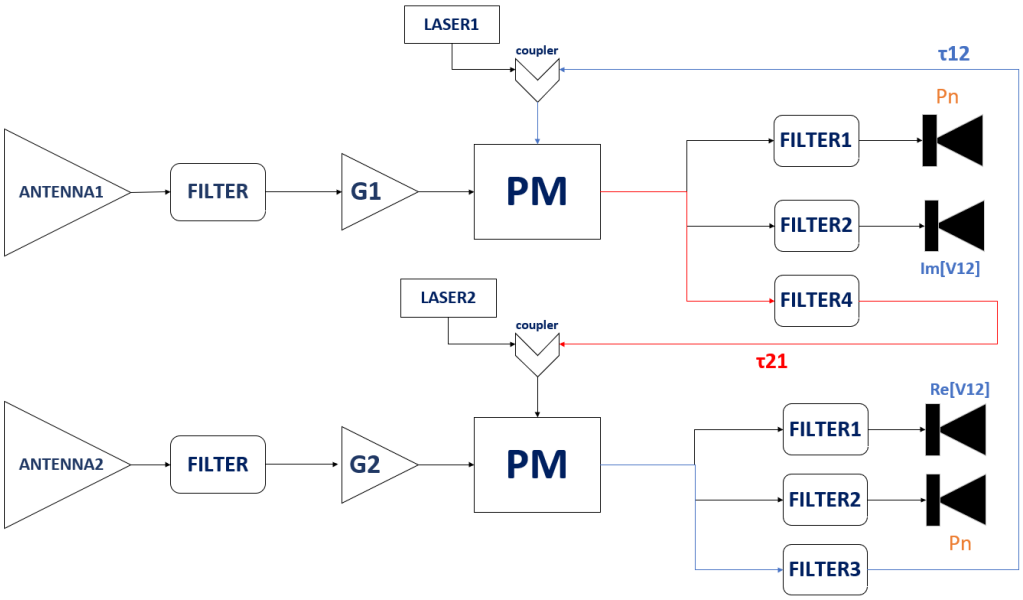

Figure 7.3 Setup that gets imaginary part and real part at the same time with double remodulation

The output of the first PM is now:

$$E_{out\ PM1}(t) = \left(E_{laser\ 1}(\omega_1, t)e^{j\alpha_1} + \frac{E_{laser\ 2}(\omega_2, t)}{\sqrt{3}} e^{j\frac{\pi\, x_{r,2}(t)}{V_\pi}} e^{j\alpha_2}\right) e^{j\frac{\pi\, x_{r,1}(t+\tau_{21})}{V_\pi}} \tag{7.20}$$

And the output of the second PM is :

$$E_{out\ PM2}(t) = \left(E_{laser\ 2}(\omega_2, t) e^{j\alpha_3} + \frac{E_{laser\ 1}(\omega_1, t)}{\sqrt{3}} e^{j\frac{\pi\, x_{r,1}(t)}{V_\pi}} e^{j\alpha_4} \right) e^{j\frac{\pi\, x_{r,2}(t+\tau_{12})}{V_\pi}} \quad (7.21)$$

Filter 3 gets the modulated signal from $E_{out\ PM2}(t)$ and is sent with a delay of τ_{21} to get remodulated in the first PM. Meanwhile, filter 4 gets the modulated signal from $E_{out\ PM1}(t)$ and is remodulated in the second PM with delay of τ_{12}.
From receiver 1 filter 1 gets the carrier and upper sidebands of the modulated signal and filter 2 gets the same but from the remodulated signal. From receiver 2 is the opposite, filter 1 gets the carrier and upper sidebands of the remodulated signal and filter 2 from the modulated signal. So by photodetecting the remodulated signals with appropiate τ_{12} and τ_{21} we can get the imaginary part and real part at the same time. The mathematics are the same as in the previous sections but we have to take into account that the distribution divides the power, the photocurrent of the remodulated signal is divided by 9 and that is only for one baseline .

An alternative for obtaining the real and imaginary parts of the visibility would be to make use of the redundant baselines see Figure 4.4, as they are in the same spatial frequency u, for identical receivers they would measure the same visibility sample.

By setting up half of the redundant baselines to $\omega_m\tau = n\,\pi\ for\ n\ odd$ or $\omega_m\tau = k\ 2\pi\ for\ k\ even$ in order to detect the real part of the visibility.

And the other half of the baselines to $\omega_m\tau = (j+1)\frac{\pi}{2}\ for\ j = 2{,}6, \ldots$ or $\omega_m\tau = (l+1)\frac{\pi}{2}\ for\ l = 0{,}4{,}8 \ldots$ for the imaginary part of the visibility.

So we don't need to use 2 remodulations per baseline as Figure 7.3 with the inconvenience of dividing that much the power of our signals.

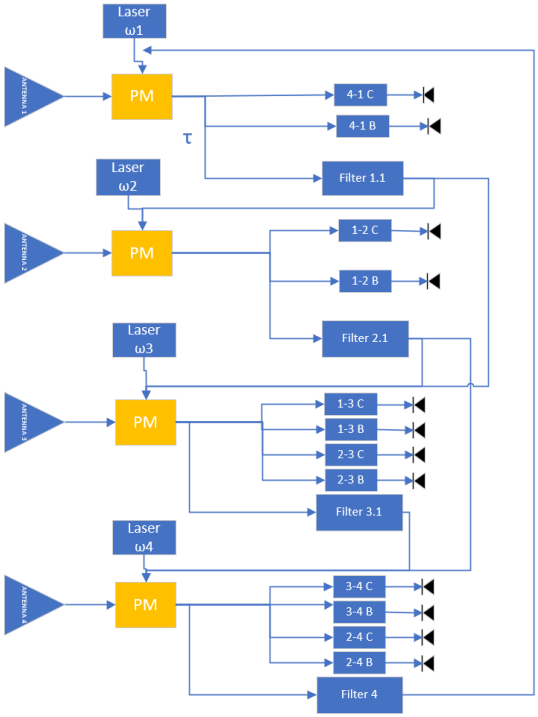

Figure 7.4 Design based on 7.1 but with 4 antennas C are filters in the remodulated signals for the crosscorrelation, and B are filters in the modulated signals for the power V_n^2.

7.2 Simulations for a point source :

In this section we simulate the initial setup 7.1. using the commercial software Optiwave. Using noise source and a band pass rectangle filter we generate $x_{r,1}(t)$ and $x_{r,2}(t)$. In order to simulate τ from the fiber and $\frac{\Delta r_i}{c}$ from the path difference to both antennas, ideal time delays are implemented. The photocurrent generated by the photodiode pin is then transmitted to Matlab where the average of this signal is done and correlations are plotted, see Figure 7.5.

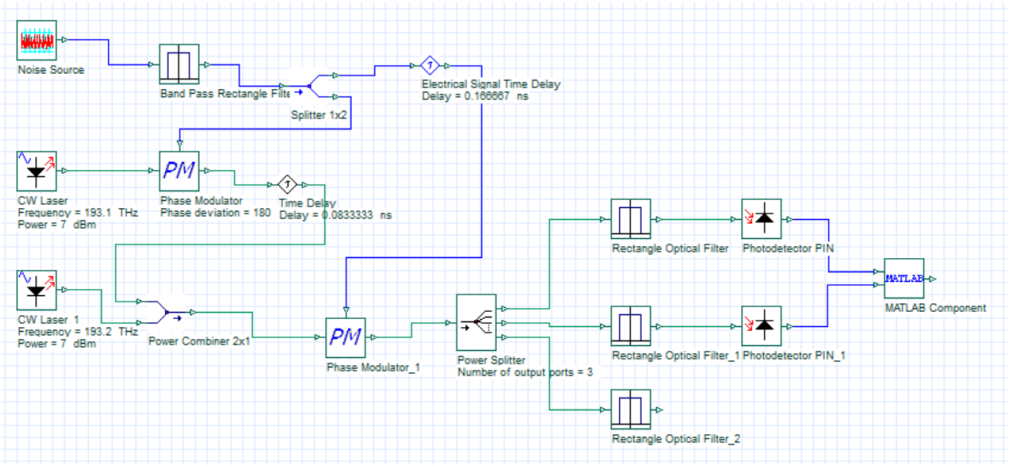

Figure 7.5 Scheme of the simulation done with Optisystem 15.

The integration time is defined in the software as the time window, which is the total amount of time it is sampling:

$$T_{window} = \frac{Sequence\ length}{Bit\ Rate}$$

Working with a speed of $10^9 bits/s$ and a sequence length of 512 bits, we got an integration time of $T_{window} = 0.512\mu s$. The quality of the results are given also by the $\frac{sample}{bit}$, in this case we use 128 so we got a number of samples $N_{samples} = \frac{sample}{bit} x\ Sequence\ length = 65536$ which was enough for all the simulations done, see Figure 7.6

Simulation | Signals | Spatial effects | Noise | Signal tracing

Name	Value	Units	Mode
Simulation window	Set bit rate		Normal
Reference bit rate	☑		Normal
Bit rate	1000000000	Bits/s	Normal
Time window	5.12e-007	s	Normal
Sample rate	128000000000	Hz	Normal
Sequence length	512	Bits	Normal
Samples per bit	128		Normal
Number of samples	65536		Normal

Figure 7.6 Simulation parameters used

Remember from section 5 that the index of modulation has to be low so higher orders of the Taylor approximation used are negligible. We use an index of modulation of about $m = \frac{\pi}{V_\pi} V_{rf} \approx 0.20$ in all the simulations, and we checked have that results doesn't change much in the range $0.10 \leq m \leq 0.4$. If $m < 0.10$ higher order terms are negligible but the sideband powers are so low that the system doesn't detect it at all. If $m > 0.4$ higher order terms starts to get important so the design starts to fail.

The following simulations are done for a baseline of $u = \frac{1}{2}$, where $f_m = 3GHz$, a bandpass filter of $B = 100MHz$. We simulate a point source that moves from $(\xi_1, \xi_2) = (-0.1, 0.1)$, so the phase difference between both antennas $\Delta\theta = f_m \frac{\Delta r_i}{c} 360$ will change from $-180\ to\ 180$ degrees.

By changing τ manually we get the real part and imaginary part, that is 7.18 and 7.19 respectively. Using $\tau_i\ \omega_m = \frac{\pi}{2}$ for the imaginary part and $\tau_r\ \omega_m = 2\pi$ for the real part, we get the results in Figure 7.7 :

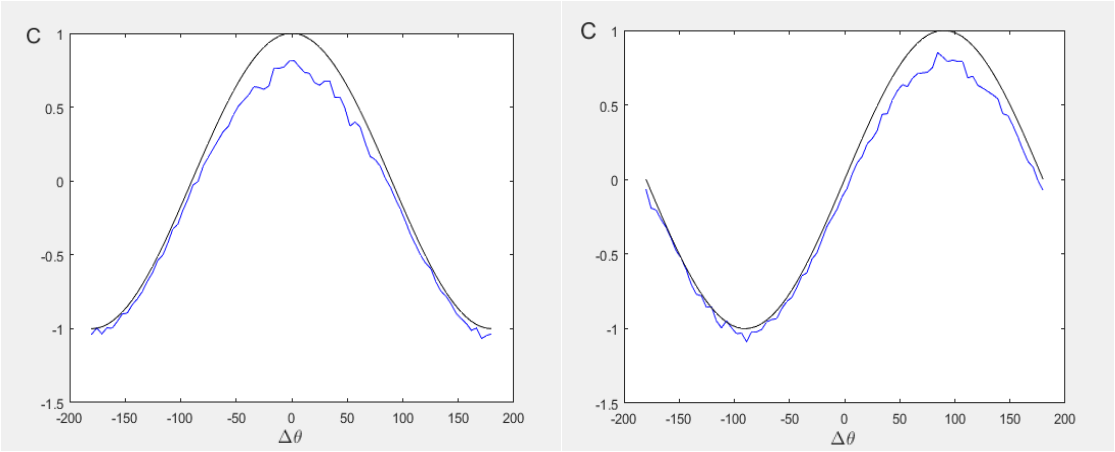

Figure 7.7 Blue and black are respectively simulation and theoretical results. Shown in the left hand side are results for the real part ($\tau_r = 0.333ns$) of the correlation while the right hand side is for the imaginary part($\tau_i = 0.0833ns$) .

For positive angles the correlations have significant errors. This is intrinsic to the design, from equation (7.16) we deduce that whenever the photodiode starts to reduce its value, it is going to introduce errors. If we use $\tau_i\ \omega_m = \frac{3\pi}{2}$ for the imaginary part and $\tau_r\ \omega_m = \pi$ for the real part, the photodiode starts to reduce its value for negatives angles and the error is going to appear for the negatives angles see Figure 7.8.

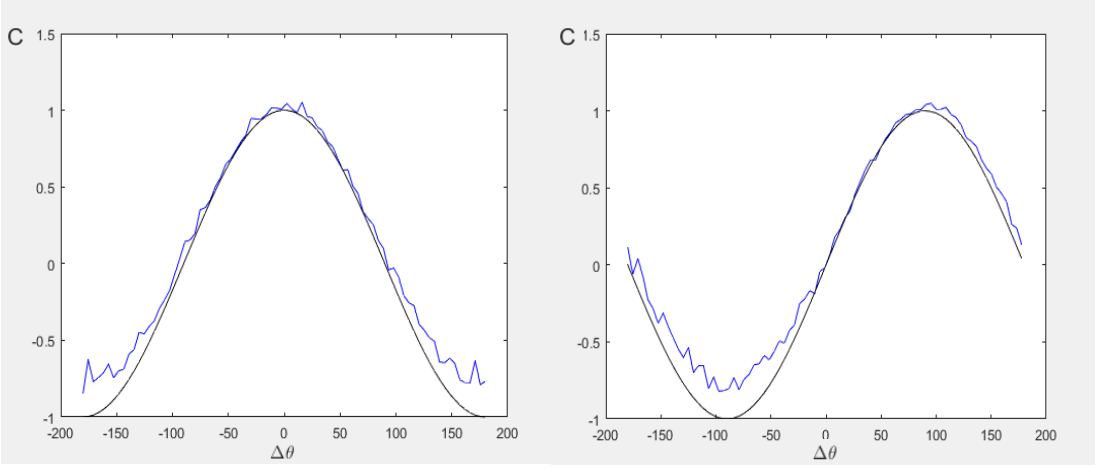

Figure 7.8 Simulation results showing errors in the negative angles. $\tau_r = 0.1666ns$ for the left hand side and $\tau_i = 0.25ns$ for the right hand side

As $\frac{\Delta r_{max}}{c} = -0.1666ns$, and $\tau_{max} = 0.3333ns$ we do not suffer from decorrelation effects because from 7.18 $sinc_N\left(B\left(\frac{-|\Delta r_{max}|}{c} - \tau_{max}\right)\right) \approx 1$.

If we implement a simple algorithm for the design consisting that in case we detect negative $\Delta\theta$ we use the correlations of the redundant baselines with $\tau_i\ \omega_m = \frac{\pi}{2}\ and\ \tau_r\ \omega_m = 2\pi$, and if we detect positive $\Delta\theta$ we can use the correlations of the rest

redundant baselines with $\tau_i = \frac{3\pi}{2}\ and\ \tau_r = \pi$. The results of this strategy are shown in Figure 7.9.

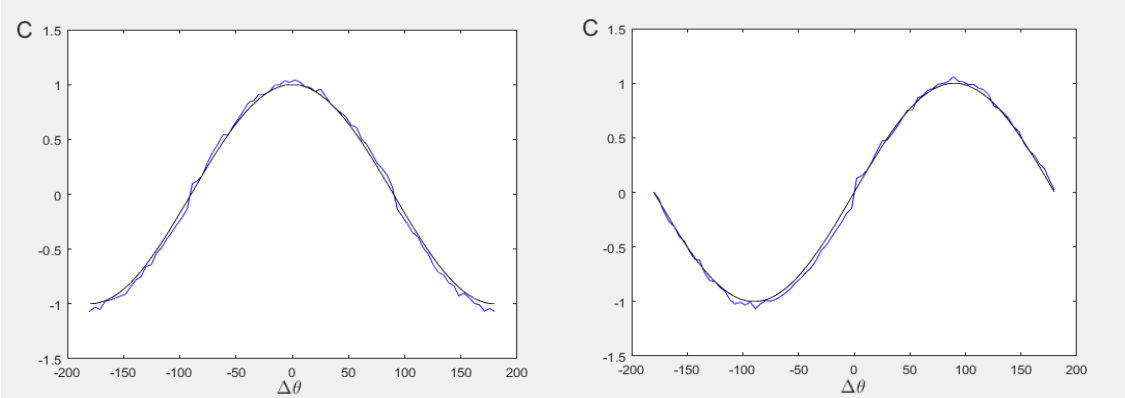

Figure 7.9 Results using redundacy of the baselines

Next, results in order to show decorrelation effects are presented using redundacy strategy, that is by using higher bandwidth $B = 1GHz$, baseline $\Delta x = 0.5m$, $f_m = 3GHz$, and $\tau = 0.1666ns$. If simulating a point source that moves from $(\xi_1, \xi_2) = (-0.4, 0.4)$:

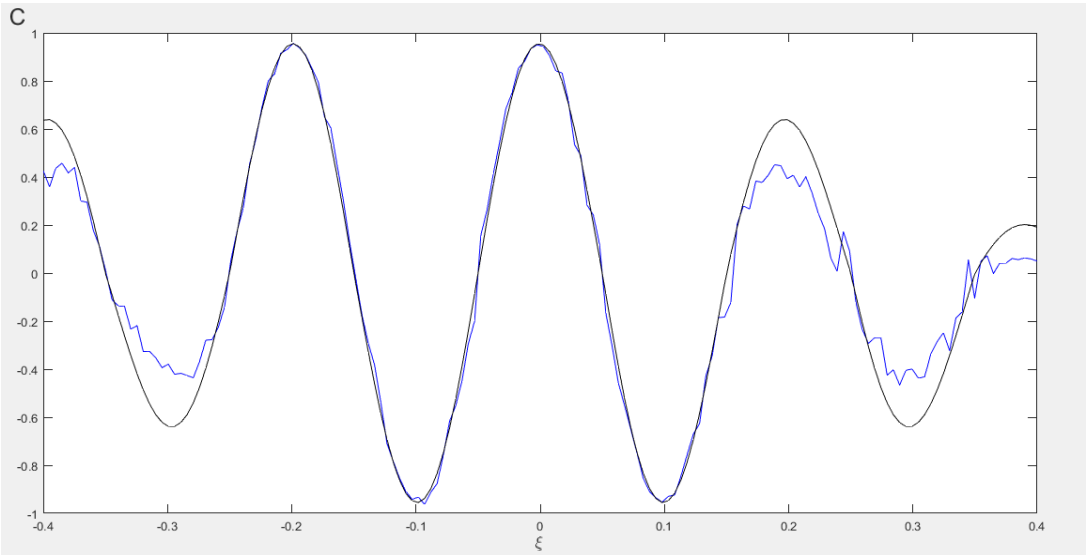

Figure 7.10 Simulation results showing decorrelation effect with redundancy technique

We can see that if the signal comes from the right $\xi > 0$, we are going to loose more information than if it comes from the left. That is because if the signal arrives first to the first antenna, the time delay because of antenna position helps the system to syncronize a little bit . However the system is not robust under hard decorrelation effects.

By reducing the Bandwidth to 50MHz and by implementing a τ equivalent of the baseline length , that is $\tau = 3.3333\ ns$ we got very low decorrelation effects:

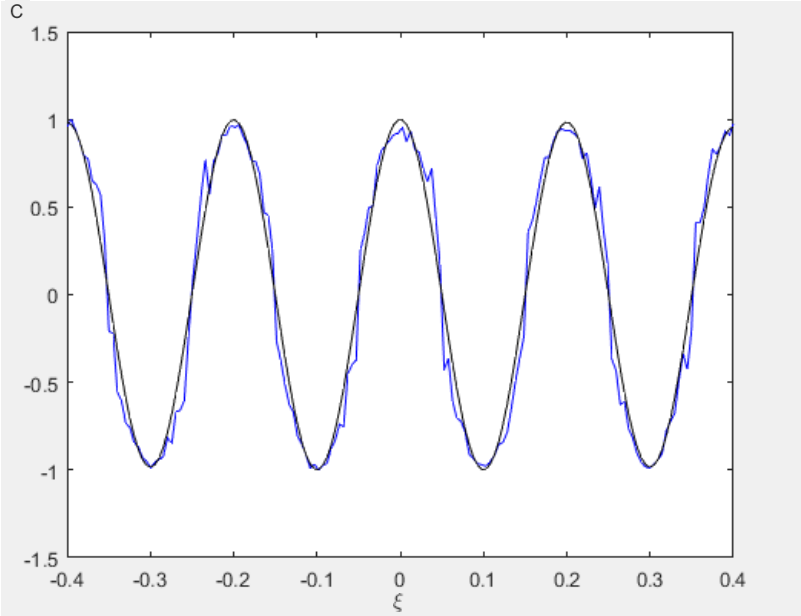

Figure 7.11 Simulation results without decorrelation

For an extended source this result wouldn't be that good, as there will be inifinitessimal points from the source coming with positive and negative phase difference. By using the redundancy strategy, if we want to improve the results we need at least 4 redundant baselines.

For the real part of the visibility if we setup one redundant baseline to $\omega_m \tau_{1,r} = n\pi \; for \; n \; odd$, and the second redundant baseline to $\omega_m \tau_{2,r} = k2\pi \; for \; k \; even$. The same as for the imaginary part of the visibility if the third baseline applies $\omega_m \tau_{3,i} = (j+1)\frac{\pi}{2} \; for \; j = 2,6, \ldots$ and the fourth one $\omega_m \tau_{4,i} = (l+1)\frac{\pi}{2} for \; l = 0,4,8 \ldots$

By measuring the visibilities of the redundant baselines, the errors on both positive and negative angles can be averaged and we will get a better result although it won't be corrected.

In this design we face 2 though problems. On the one hand, the decorrelation effect caused by the fiber τ, which also reduces our integration time because waiting for those signals to arrive to the other PM is needed. On the other hand, bad results either for positive or negative angles depending on tau, which is intrinsic in the design, and will be difficult to correct for extended sources.

7.3 Synchronization of signals

A possible method in order to compensate this τ is by synchronizing the signals using a second EOM stage as depicted in Figure 7.12 :

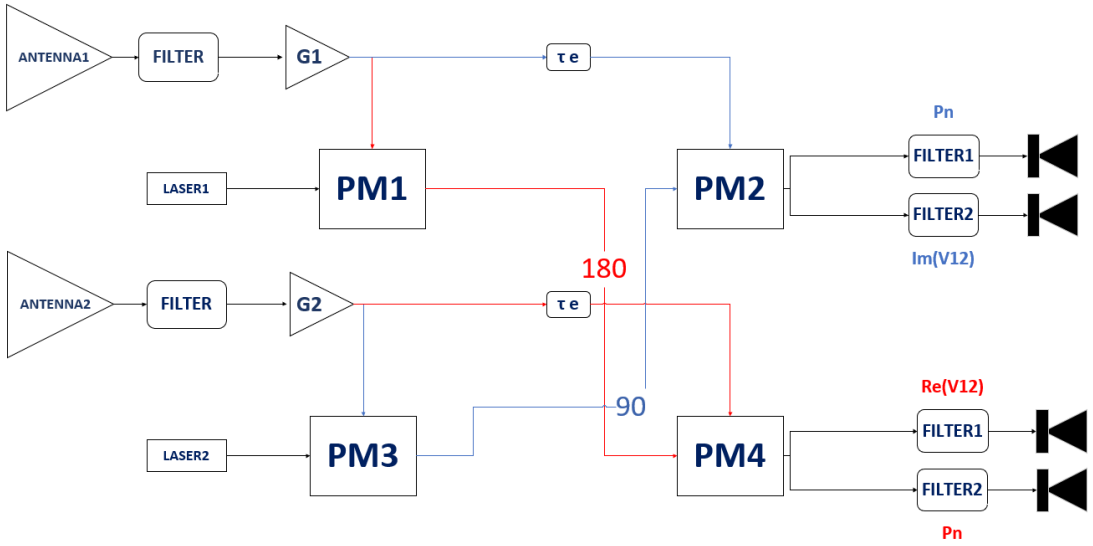

Figure 7.12 Scheme of the synchronization technique doubling the number of phase modulators.

It consists in upconverting 2 times the RF signal with 2 PM (one time per PM) per receiver in order to synchronize the signals. Focusing in the first receiver, laser1 from PM1 is modulated by the RF signal $x_1(t)$ and is sent with fiber marked in red to PM4 of the second receiver where is remodulated hence correlated with $x_2(t)$. The synchronization of both signals is done with the electrical delay τ_e that compensates the path between PM1 and PM4 so both signals can arrive at the same time at PM4.

In order to get the real part or the imaginary part, we can add a very little τ with respect to the τ_e, so if $(\tau_e - \tau_{fiber})\ \omega_m = \pi \ \ or\ 2\pi$ we get the real part of the visibility, and if $(\tau_e - \tau_{fiber})\ \omega_m = \pi/2 \ \ or\ 3\pi/2$ we get the imaginary part of the visibility.

However τ_e should be fixed for the PM N - PM M of the longest baseline N-M so all the signals can be synchronized at the same time. This is a disadvantage because in order to compensate a baseline of 7 meters, we need an equivalent electrical delay of 7 meters for every single correlation, which may need a large transmission line.

Next we show some of the basic characteristics of the design without synchronization and with synchronization in the following table.

Method	Frequency (Ghz)	B(Mhz)	Δx_{max} (m)	τ_{12} (ns)	FOV $(\Delta\xi)$	$\Delta\theta$ Resolut. (°)	Decorrelation (%)
1st	75	50	0.5	3.9	0.8	0.275	8.36
1st	75	40	0.5	3.9	0.8	0.275	5.4

1st	75	30	0.5	3.9	0.8	0.275	3.06
1st	75	20	0.5	3.9	0.8	0.275	1.37
Sync	75	200	0.5	0.0066	0.8	0.275	2.96
Sync	75	150	0.5	0.0066	0.8	0.275	1.67
Sync	75	100	0.5	0.0066	0.8	0.275	0.74
Sync	75	50	0.5	0.0066	0.8	0.275	0.19
1st	1,2	20	6	30	0.8	1.432	71.33
1st	1,2	10	6	30	0.8	1.432	22.12
1st	1,2	5	6	30	0.8	1.432	5.83
1st	1,2	2	6	30	0.8	1.432	0.95
Sync	1,2	40	6	0.4166	0.4	1.432	5.06
Sync	1,2	30	6	0.4166	0.4	1.432	2.8
Sync	1,2	20	6	0.4166	0.4	1.432	1.28
Sync	1,2	10	6	0.4166	0.4	1.432	0.32

Table 7.1 Method 1st is the technique of the figure 7.1, and method Sync is the technique using synchronization of the signals in 7.12. Here we propose 2 frequencies one at 75GHz, and 1.2 Ghz .

Decorrelation effect is for the worst scenario , a source coming from the edge of the FOV to the longest baseline.

Working at low microwave frequencies 1.2GHz , we need a larger baseline in order to get decent resolution. But we get hard decorrelation effects, a possible solution would be decreasing the FOV , so it will take more time for the satellite to recover the Earth's brightness map. An advantage can be that we can improve the sensitivity by improving the bandwidth as after decreasing the FOV we are able to do that.

If using 75 GHz , we don't need large baselines, so decorrelation effects will be relatively lower. However the τ_{12} is still very annoying as it limits our bandwidth to 20-40 MHz. With synchronization technique we can jump to 150 MHz highly improving the sensitivity of the system, with the disadvantage of adding complexity and doubling the cost of the system .

7.4 EXPERIMENTAL SETUP

Figure 7.13 shows the scheme of the experimental setup built in our laboratory. By using a network analyzer , we generate a monochromatic signal at 12.5GHz with an amplitude of Vrf=480mV. The RF signal goes into a power splitter where is divided in 2, one goes to a phase shifter which will simulate the phase difference between the 2 antennas of one baseline, and the other one will remain the same.

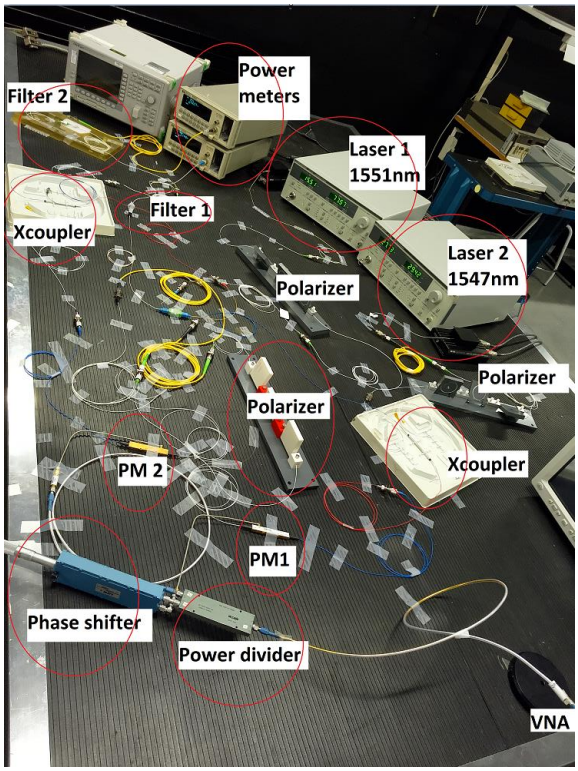

Figure 7.13 Schematic of the experimental setup in the laboratory

The shifted signal will modulate the DFB Laser at 1547nm with the first phase modulator (PM1). The unchanged RF signal will remodulate the output of PM1 and modulate the second DFB laser at 1551nm in the second phase modulator (PM2).

The DFB lasers come in a butterfly casing and are connected to temperature and current controls in order to select respectively the output wavelength and power.

The output of PM2 is going to be splitted in two with a Xcoupler and by using filter 1 we get the remodulated signal (which carries information of the cross terms) and filter 2 to get the modulated signal which is proportional to $\frac{\pi V_{rf}}{2V_{\pi}}$. The response of both filters are :

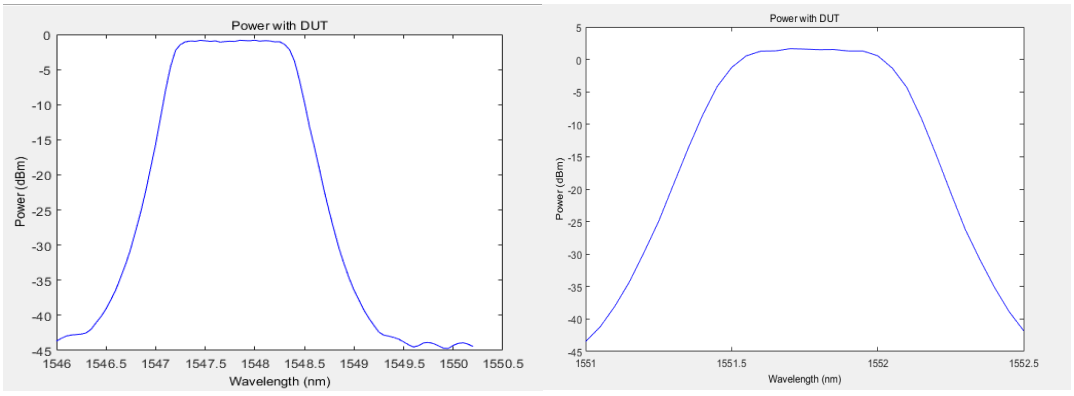

Figure 7.14 Response of the filters used in the experimental setup, in the left hand side Filter 2 and the right hand side Filter 1 .

In order to detect the power of the modulated signal and the remodulated signal, we have used two power detectors from Hewlett Packard (HP) series 8153, with an uncertainty of about $\pm 5\ pW$ which is irrelevant for our experiments.

The two phase modulators used are the model LN27S-FC rom Thorlabs, whose characteristics are summarized in table 7.2:

Operating frequency range	DC-40Ghz
Operating wavelength	1525nm-1605nm
Max RF input power	24dBm
Max operating temperature	75 centigrades
V_π	7.5 V

Table 7.2 characteristic parameters of the PM used in the experiments

With Vrf=480mV, we should have an index of modulation approximately of :

$$m = \frac{\pi V_{rf}}{V_\pi} = 0.2$$

Here we faced 4 main difficulties.

1- The RF power splitter is not exact, and the index of modulation in the first modulator is going to be different to the one in the second modulator. But in the calibration process we can determine the values of both modulation indices, m and m' in order to compensate this error.

2- When moving the phase shifter between 0 and 360 degrees in order to simulate a moving point source, the phase shifter produces a high reflection that affects to the other output of the power splitter introducing phase errors on the order of 1-9 degrees, so we are not going linearly from 0 to 360 degrees. In a practical case, the delayed signal would come from different antennas, and no phase shifter would be present.

3- The PM may have a fiber with bad conditions, it introduces an oscillation of about 0.05µW. in spite of that, the system is robust in front of these oscillations.

4- Also, from the PM there is a bias drift associated with the change of the $V_\pi(t)$ which decalibrates our system.

5- Filters are not as narrow as we want, calibration should be very precise to compensate different insertion loss seen by different spectral components.

While 1,5 are compensated with good calibration, 2,3 and 4 couldn't be fixed so lab results will carry those errors.

Calibration process :

In order to filter in the carrier and USB, the filter implemented is not perfect and our

sidebands and carriers will be attenuated by different factors so a calibration process is needed.

As we are dealing with a monochromatic source, we can use the expressions from (7.3) and with Bessel expansion from (5.3), the remodulated signal is :

$$E_{rem}(t) = E_0 e^{j(\omega_1 t+\theta_1)} e^{j\alpha_1}\left(\beta_0 + j\beta_1 e^{j(\omega_{rf}t+\phi_1)} + j\beta_1 e^{-j(\omega_{rf}t+\phi_1)}\right)\left(\beta_0' + j\beta_1' e^{j(\omega_{rf}(t+\tau)+\phi_2)} + j\beta_1' e^{-j(\omega_{rf}t+\tau)+\phi_2)}\right) \quad (7.22)$$

After filtering we have :

$$E_{filt\ 1}(t) = \frac{E_0}{\sqrt{C_{tot}}} e^{j(\omega_1 t+\theta_1)} e^{j\alpha_1}\left(\frac{\beta_0\beta_0' + \beta_1\beta_1' \cos(\Delta\phi+\omega_{rf}\tau)}{\sqrt{Cc}} + \frac{j\beta_0'\beta_1 e^{j\left(\omega_{rf}t+\phi_1\right)} + j\beta_1'\beta_0 e^{j\left(\omega_{rf}(t+\tau)+\phi_2\right)}}{\sqrt{C_{USB}}} + \frac{j\beta_1\beta_0' e^{-j\left(\omega_{rf}t+\phi_1\right)} + j\beta_1'\beta_0 e^{-j\left(\omega_{rf}(t+\tau)+\phi_2\right)}}{\sqrt{C_{LSB}}}\right) \quad (7.23)$$

Note that we assumed that the modulated signal at ω_2 is negligible because it is at 45dB lower due to filter1.

So the photodetected signal is :

$$I_{ph}(\Delta\phi) = \frac{E_0^2}{C_{tot}}\left(\frac{1-2\beta_1'^2-2\beta_1^2-4\beta_1\beta_1' \cos(\Delta\phi+\omega_{rf}\tau)}{Cc} + \left(\beta_1'^2 + \beta_1^2 + 2\beta_1\beta_1' \cos\left(\Delta\phi + \omega_{rf}\tau\right)\right)\left(\frac{1}{C_{USB}} + \frac{1}{C_{LSB}}\right)\right) \quad (7.24)$$

Cc, C_{USB}, C_{LSB} are measured by disconnecting the RF signal, and calculating the attenuation at f_0+f_m, f_0 and f_0-f_m. $\frac{E_0^2}{C_{tot}}$ is the total power taking into account all the attenuation of the receiver chain (fiber transitions, connectors etc…) and is referenced at the bandpass of the filter.

For $f_m = 12.5GHz$:

Cc	4.5276
C_{USB}	26.9975
C_{LSB}	1.3396
$\frac{E_0^2}{C_{tot}}$	86’419 µW

Table 7.3 Coefficients of attenuation in each sideband ,carrier and the referenced power of the laser

$\beta_1\ and\ \beta_1'$ are different because the power splitter isn’t perfect as discussed previously. In order to measure them what is done in the lab is the following :

If we disconnect from the second PM's the RF signal we can get β_1, so instead of getting the correlations with filter 1 we would get this power. Remember that β_1' has no problem because it is measured directly with the second filter. So we get a linear relation between β_1' and β_1 which theoretically has to be maintained.

For Vrf=480mV we got :

β_1	0.1243
β_1'	0.0986

Table 7.4 First order measured Bessel coefficients from each PM

As we can see, the voltage attenuated in the second PM due to the phase shifter and power divider imperfections, is relatively 26% more in this second PM.

Next results without measuring τ are shown, starting from the mean value of $I_{ph}(\Delta\phi)$, that is $\Delta\phi_0 + \omega_{rf}\tau = \frac{\pi}{2}$,so we will measure the imaginary part of the correlation. By changing $\Delta\phi$ from $\Delta\phi_0$ with the phase shifter we see that the measured $I_{ph}(\Delta\phi)$ has an sinusoidal form with amplitude of $1.5\mu W$. By Isolating the $\cos(\Delta\phi + \omega_{rf}\tau)$ from this $I_{ph}(\Delta\phi)$ we get the following results:

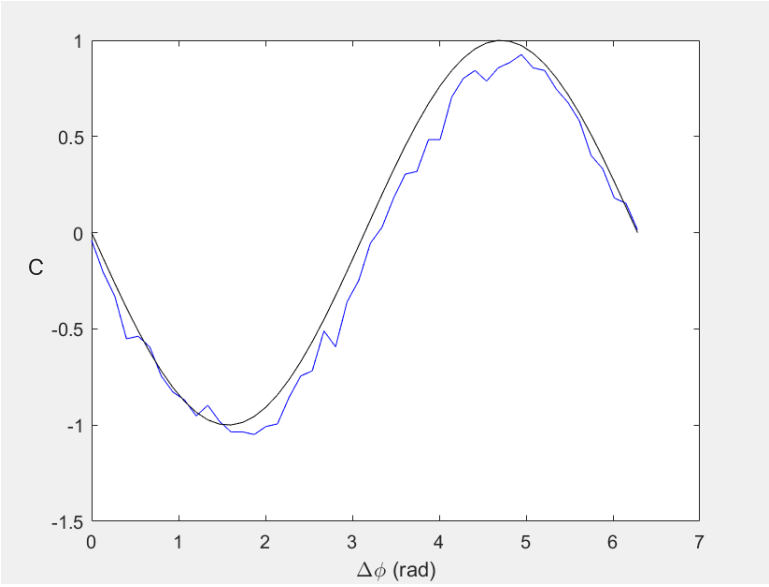

Figure 7.15 Measured imaginary part of the normalized visibility as a function of phase shifter angle in radians for a point source

The result in Figure 7.15 proves the calibration process and validates that the visibility function for a point source can be extracted from measurements of the power of the remodulated and modulated signal.

8.Conclusions

In this work we have presented a review of the main definitions regarding passive Synthetic aperture radiometers in the microwave band focused to Earth Observation applications from Low orbit satellites such as SMOS.

The main definitions and relationships regarding Brightness Spectral Function, Brightness temperature, Field of View, coherence, etc, have been derived from basic principles.

The study has allowed to assess the potential of photonics for Synthetic Aperture radiometry in the microwave band. In this regard, several photonic microwave radiometer proposals have been reviewed. An in-depth advantages/challenges analysis has allowed to derive a new proposal based on electro-optical remodulation, which has been described in detail and theoretically justified.

The design of our photonic correlator using remodulation technique was successfully proved for a point source. The advantage of avoiding feedback loop compensation costed the extra decorrelation effect due to the additional path from one receiver to the other, which also reduces our acquisition time hence the sensitivity of the system. A second photonic microwave radiometer proposal aims at overcoming this problem by doubling the number of phase modulators.

Even if the cost of the system will significantly increase, it may be justified by better performance while avoiding bandwidth-limited feedback loops or costly custom integrated optics.

In addition, we have seen that the intrinsic problem of the design that affects the measured correlations of extended sources depending if the target emission arrives from a positive or negative angle may be improved when using redundancy and averaging them.

With respect to the optical filtering, it is challenging to optically filter sidebands with less than 5GHz distance. A possible solution to that would be to use a frequency shift technique by means of a dual drive Mach Zehnder amplitude modulator, where applying a specific bias voltage and RF shift between the 2 electrodes of the modulator, we can cancel out the LSB no matter at which RF frequency [11]. That would be a line of research worth exploring in future works.

The experimental part of this thesis proved the new photonic correlator proposals for a one point source moving scenario. We used a RF frequency of 12.5GHz in order to cancel out the USB as much as possible using optical filtering, but we realized that it also worked for 5GHz with appropriate calibration. We noticed the effect of the Bias drift of the phase modulator, which is a $V_\pi(t)$ that may decalibrate a little bit the system. Although it is very slow and doesn't affect very much the results, it should be compensated.

In conclusion, the design of the photonic correlator of this thesis may be used for working in high frequencies where no long baselines are needed hence being far from the limit of decorrelation effects. In order to improve the sensitivity, the synchronization technique can be used in order to extend the bandwidth of operation. Future works for improving this prototype would be an in depth study of errors, and experiments with extended sources and actual antennas.

9. APPENDIX

Appendix 1 - GENERIC PARSEVAL'S THEOREM

The cross correlation function for a finite power process is defined as:

$$R_{xy}(\tau) = \int_{-\infty}^{+\infty} x(t)y^*(t-\tau)dt$$

which is equivalent to a convolution :

$$R_{xy}(\tau) = x(\tau) * y^*(-\tau) = \int_{-\infty}^{+\infty} x(t)y^*\big(-(\tau - t)\big)dt = \int_{-\infty}^{+\infty} x(\tau)y^*(t-\tau)dt$$

$$F\left(R_{xy}(\tau)\right) = X(f)\, Y^*(f)$$

$$R_{xy}(\tau) = F^{-1}\big(X(f)\, Y^*(f)\big) = \int_{-\infty}^{+\infty} X(f)\, Y^*(f) e^{j2\pi f\tau} df$$

As τ = 0 , the time domain cross correlation at the origin, is equivalent to :

$$R_{xy}(0) = \int_{-\infty}^{+\infty} x(\tau)y^*(t)dt = \int_{-\infty}^{+\infty} X(f)\, Y^*(f)\, df$$

Which is the generic Parseval's theorem .

In our process, would not converge as it is an integral going from $-\infty$ to ∞. So we average it by the integration time T, but the rest of equalities are equivalent.

$$R_{xy}(0) = \lim_{T\to\infty} \frac{1}{T} \int_{-\frac{T}{2}}^{\frac{T}{2}} x(t)y^*(t)dt = \int_{-\infty}^{+\infty} X(f)Y^*(f)df$$

APPENDIX 2 – THE FILTERED REMODULATED SIGNAL

- The output of the second modulator is by assuming identical receivers $x_{r,2}(t) = x_{r,1}\left(t - \frac{\Delta r}{c} + \tau\right)$ and by substituting it by the equivalent noise model :

$$x_{r,i}(t) = Re\left(n_i(t)\, e^{j\omega_m t} \right) \text{ with } n_i(t) = n_{Ii}(t) + jn_{Qi}(t)$$

The output of the PM2 is then :

$$\begin{aligned} E_{outPM2}(t) = E_0 e^{j(\omega_1 t+\theta_1)} e^{j\alpha_1} \Bigg(& 1 + j\frac{\pi}{V_\pi} x_{r,1}(t) + j\frac{\pi}{V_\pi} x_{r,1}\left(t - \frac{\Delta r}{c} + \tau\right) \\ & - \frac{1}{2}\left(\frac{\pi}{V_\pi}\right)^2 \left(x_{r,1}(t)^2 + x_{r,1}\left(t - \frac{\Delta r}{c} + \tau\right)^2 \right) \\ & - \left(\frac{\pi}{2V_\pi}\right)^2 \Bigg(n_{I1}(t) n_{I1}\left(t - \frac{\Delta r}{c} + \tau\right) \cos(\omega_m t) \cos\left(\omega_m\left(t - \frac{\Delta r}{c} + \tau\right)\right) \\ & - n_{I1}(t) n_{Q1}\left(t - \frac{\Delta r}{c} + \tau\right) \cos(\omega_m t) \sin\left(\omega_m\left(t - \frac{\Delta r}{c} + \tau\right)\right) \\ & - n_{I1}\left(t - \frac{\Delta r}{c} + \tau\right) n_{Q1}(t) \cos\left(\omega_m\left(t - \frac{\Delta r}{c} + \tau\right)\right) \sin(\omega_m t) \\ & + n_{Q1}(t) n_{Q1}\left(t - \frac{\Delta r}{c} + \tau\right) \sin(\omega_m t) \sin\left(\omega_m\left(t - \frac{\Delta r}{c} + \tau\right)\right) \Bigg) \Bigg) \\ & + E_0 e^{j(\omega_2(t+\tau)+\theta_2+\alpha_2)} \left(1 + j\frac{\pi\, x_1\left(t - \frac{\Delta r}{c} + \tau\right)}{V_\pi} - \left(\frac{\pi\, x_1\left(t - \frac{\Delta r}{c} + \tau\right)}{V_\pi}\right)^2 \right) \end{aligned}$$

So filtering carrier and USBs from the remodulated signal we have :

$$\begin{aligned} E_{rem} = E_0 e^{j(\omega_1 t+\theta_1)} e^{j\alpha_1} \Bigg(& 1 - 2\left(\frac{\pi}{2V_\pi}\right)^2 \left(n_1(t)^2 + n_1^2\left(t - \frac{\Delta r}{c} + \tau\right) \right) \\ & + j\,\frac{\pi\, n_1\left(t - \frac{\Delta r}{c} + \tau\right)}{2V_\pi} e^{j\omega_m\left(t - \frac{\Delta r}{c} + \tau\right)} + j\frac{\pi\, n_1(t)}{2V_\pi} e^{j\omega_m t} \\ & - 2\left(\frac{\pi}{2V_\pi}\right)^2 Re\left(n_1(t) n_1^*\left(t - \frac{\Delta r}{c} + \tau\right) e^{j\omega_m\left(\frac{\Delta r}{c} - \tau\right)} \right) + O^3 \Bigg) \end{aligned}$$

APPENDIX-3 SUPERPOSITION FOR INCOHERENT SOURCE IN A PHOTONIC CORRELATOR

In order to simplify notations, we will expand with Taylor but just until first order and supposing that $\alpha_1 = \alpha_2 = 0$. For a simple demonstration consider the case of receiving two different points from the source :

The output from each PM is :

$$E_1(t) = A\, e^{j(\omega_0 t+\theta_1)}\left(1 + j\frac{\pi\, x_{r,1}(\overline{r_1},t)}{V_\pi} + j\frac{\pi\, x_{r,1}(\overline{r_2},t)}{V_\pi}\right) \;\; ; \;\; E_2(t) = Ae^{j(\omega_0 t+\theta_1)}\left(1 + j\frac{\pi\, x_{r,2}(\overline{r_1},t)}{V_\pi} + j\frac{\pi\, x_{r,2}(\overline{r_2},t)}{V_\pi}\right)$$

$\overline{r_1}$ is the position of point 1 and $\overline{r_2}$ is the position of point 2 .

After coupling we have:

$$E_{coupled}(t) = E_1(t) + E_2(t)$$

By substituting $x_{r,i}(\overline{r_j},t)$ by the equivalent model $x_{r,i}(\overline{r_j},t) = Re\left(\, n_i(\overline{r_j},t)\, e^{j\omega_m t}\right)$, and assuming identical receivers :

$$x_{r,2}(\overline{r_1},t) = x_{r,1}\left(\overline{r_1}, t - \frac{\Delta r_1}{c}\right); \quad x_{r,2}(\overline{r_2},t) = x_{r,1}\left(\overline{r_2}, t - \frac{\Delta r_2}{c}\right)$$

Filtering the carrier and USBs of $E_{coupled}(t)$ we have :

$$E_{filtered}(t) = 2 + j\frac{\pi}{2V_\pi}e^{j\omega_m t}\left(n_1(\overline{r_1},t) + n_1(\overline{r_2},t)\right) + j\frac{\pi}{2V_\pi}n_1\left(\overline{r_1}, t - \frac{\Delta r_1}{c}\right)e^{j\omega_m\left(t-\frac{\Delta r_1}{c}\right)} + j\frac{\pi}{2V_\pi}n_1\left(\overline{r_2}, t - \frac{\Delta r_2}{c}\right)e^{j\omega_m\left(t-\frac{\Delta r_2}{c}\right)}$$

Photodetecting $E_{filtered}(t)$ the instanteaneous current generated by the photodetector is :

$$I(t) = \left\|E_{filtered}(t)\right\|^2 = A^2(\,4 + \left(\frac{\pi}{2V_\pi}\right)^2\left(\|n_1(\overline{r_1},t)\|^2 + \|n_1(\overline{r_2},t)\|^2 + \left\|n_1\left(\overline{r_1}, t - \frac{\Delta r_1}{c}\right)\right\|^2 + \left\|n_1\left(\overline{r_2}, t - \frac{\Delta r_2}{c}\right)\right\|^2\right)$$
$$+2\left(\frac{\pi}{2V_\pi}\right)^2 Re(\, n_1(\overline{r_1},t)n_1^*(\overline{r_2},t) + n_1\left(\overline{r_1}, t - \frac{\Delta r_1}{c}\right)n_1^*\left(\overline{r_2}, t - \frac{\Delta r_2}{c}\right)e^{j\omega_m\frac{\Delta r_2 - \Delta r_1}{c}} + n_1(\overline{r_1},t)n_1^*\left(\overline{r_1}, t - \frac{\Delta r_1}{c}\right)e^{j\omega_m\frac{\Delta r_1}{c}}$$
$$+n_1(\overline{r_1},t)n_1^*\left(\overline{r_2}, t - \frac{\Delta r_2}{c}\right)e^{j\omega_m\frac{\Delta r_2}{c}} + n_1(\overline{r_2},t)n_1^*\left(\overline{r_1}, t - \frac{\Delta r_1}{c}\right)e^{j\omega_m\frac{\Delta r_1}{c}} + n_1(\overline{r_2},t)n_1^*\left(\overline{r_2}, t - \frac{\Delta r_1}{c}\right)e^{j\omega_m\frac{\Delta r_2}{c}}\,))$$

As the source is incoherent, the cross correlation between two different points is going to be 0 so the average of $I(t)$ is :

$$\overline{I(t)} = A^2\,[\,4 + \left(\frac{\pi}{2V_\pi}\right)^2\frac{1}{T}\int_T \|n_1(\overline{r_1},t)\|^2 + \|n_1(\overline{r_2},t)\|^2 + \left\|n_1\left(\overline{r_1}, t - \frac{\Delta r_1}{c}\right)\right\|^2 + \left\|n_1\left(\overline{r_2}, t - \frac{\Delta r_2}{c}\right)\right\|^2 dt +$$
$$2\left(\frac{\pi}{2V_\pi}\right)^2 Re\left(\frac{1}{T}\int_T n_1(\overline{r_1},t)n_1^*\left(\overline{r_1}, t - \frac{\Delta r_1}{c}\right)e^{j\omega_m\frac{\Delta r_1}{c}} + n_1(\overline{r_2},t)n_1^*\left(\overline{r_2}, t - \frac{\Delta r_1}{c}\right)e^{j\omega_m\frac{\Delta r_2}{c}}\, dt\right)\,]$$

If we want to take into account all the points from the extended source then as we can see in previous equation it can be done by superposition, that is :

$$\frac{\overline{I(t)}}{A^2} = 4 + \left(\frac{\pi}{2V_\pi}\right)^2 \frac{1}{T}\int_T \overline{\|n_1(\overline{r_i},t)\|^2} + \overline{\left\|n_1\left(\overline{r_i},t-\frac{\Delta r_i}{c}\right)\right\|^2} + 2Re\left(\overline{n_1(\overline{r_i},t)n_1^*\left(\overline{r_i},t-\frac{\Delta r_i}{c}\right)e^{j\omega m\frac{\Delta r_i}{c}}}\right)\,dt$$

So the design of a photonic correlator can be carried out for a point source and generalize it for an extended by simple superposition.

If we average these 3 terms from the previous equation

$\frac{1}{T}\int_T \overline{\|n_1(\overline{r_i},t)\|^2 dt} = \frac{1}{T}\int_T \sum_{i=1}^{N}\|n_1(\overline{r_i},t)\|^2 dt = \iint_{4\pi}\frac{k_B\,G\,R_a}{\Omega}T_B(\theta,\varphi)t(\theta,\varphi)\,d\Omega$ is the

baseband noise power received by the first antenna.

And

$$\frac{1}{T}\int_T \overline{\left\|n_1\left(\overline{r_i},t-\frac{\Delta r_i}{c}\right)\right\|^2}\,\mathrm{dt} = \frac{1}{T}\int_T \sum_{i=1}^{N}\left\|n_1\left(\overline{r_i},t-\frac{\Delta r_i}{c}\right)\right\|^2 dt = \iint_{4\pi}\frac{k_B\,G\,R_a}{\Omega}T_B(\theta,\varphi)t(\theta,\varphi)\,d\Omega$$

is the baseband noise received by the second antenna, they are the same because identical receivers was assumed.

The average of the cross terms is the baseband crosscorrelation (See appendix 4):

$$\frac{1}{T}\int_T \overline{n_1(\overline{r_i},t)n_1^*\left(\overline{r_i},t-\frac{\Delta r_i}{c}\right)e^{j\omega_m\frac{\Delta r_i}{c}}}\,dt = \frac{1}{T}\int_T \sum_{i=1}^{N} n_1(\overline{r_i},t)n_1^*\left(\overline{r_i},t-\frac{\Delta r_i}{c}\right)e^{j\omega_m\frac{\Delta r_i}{c}}dt = V_{12}k_B\,G\,R_a$$

APPENDIX-4 BASEBAND CROSS CORRELATION

If assuming that $n_{1,2}(t)$ are equal with a certain group delay difference [7] coming from a source point i:

$$n_2(t) = n_1\left(t - \frac{\Delta r}{c}\right)e^{-j\omega_m\frac{\Delta r}{c}}$$

The baseband cross terms $n_1(t)n_1^*\left(t - \frac{\Delta r}{c}\right)e^{j\omega_m\frac{\Delta r}{c}} = n_1(t)n_2^*(t)$.

The crosscorrelation for an extended source can be expressed as:

$$R_{n_1\,n_2}(0) = \frac{1}{T}\int_T \overline{n_1(t)n_2^*(t)}\,dt = \frac{1}{T}\int_T \overline{n_1(t)n_1^*\left(t - \frac{\Delta r}{c}\right)e^{J\omega_m\frac{\Delta r}{c}}}\,dt$$
$$= \int_{-\infty}^{+\infty}\overline{|N_1(f)|^2 e^{J\,2\pi(f_m+f)\frac{\Delta r}{c}}}\,df$$

So is equivalent of receiving $x_1(t)\ and\ x_2(t)$ but filtering from -B/2 to B/2 and cross correlating them.

Taking into account that :

$$|N_1(f)|^2 = \frac{|X_1(f)|^2|H(f)|^2}{4}$$

Where the filter is now $|H(f)|^2 = G\prod\left(\frac{f}{B}\right)$ and from section 3.17 $X_1(f) = l_{e,1}(\theta,\phi)\,X(f)$:

$$R_{n_1\,n_2}(0) = \int_{-B/2}^{B/2}\overline{\frac{G\left|l_{e,1}(\theta,\phi)\,X(f)\right|^2}{4}e^{J\,2\pi(f_m+f)\frac{\Delta r}{c}}}\,df$$
$$= \iint_{4\pi}\frac{k_B\,G\,R_a}{\Omega}T_B(\theta,\varphi)t(\theta,\varphi)\tilde{r}\left(\frac{\Delta r}{c}\right)e^{j\,2\pi f_m\frac{\Delta r}{c}}\,d\Omega = V_{12}\,k_B\,G\,R_a$$

It appears the antenna's impedance because now $x_{r,1}(t)\ and\ x_{r,2}(t)$ are not normalized voltages.

As we can see, the baseband cross correlation is the same as the cross correlation of $x_{r,1}(t)\ x_{r,2}(t)$ from section 4.27 .

$$R_{n_1\,n_2}(0) = R_{x_{r,1}\,x_{r,2}}(0) \qquad [V^2]$$

10. References

[1] Ulaby, F.T.; Moore, R.K.; Fung, A.K. Microwave remote sensing: active and passive: vols. I, II, III. Norwood, MA: Artech House, 1981-1986. ISBN 0890061939.

[2] https://www.esa.int/Our_Activities/Observing_the_Earth/SMOS

[3] P. M. Blanchard, A. H. Greenaway, A. R. Harvey, and K. Webster. Coherent Optical Beam Forming with Passive Millimeter-Wave Arrays (1999)

[4] Christopher Schuetzc, Richard Martina, Thomas Dillona, Peng Yaoa, Daniel Mackridesa, Charles Harritya, Alicia Zablockia, Kevin Shrevea, James Bonnettb, Petersen Curtb, and Dennis Pratherc Realization of a Video-Rate Distributed Aperture Millimeter-Wave Imaging System using Optical Upconversion

[5] Yuntao He, Haiping Huang, Yuesong Jiang and Yuedong Zhang. Optical phase control for MMW sparse aperture upconversion imaging

[6] Enrique Nova, Student Member, IEEE, Jordi Romeu, Fellow, IEEE, Santiago Capdevila, Student Member, IEEE, Francesc Torres, Senior Member, IEEE, and Lluis Jofre, Fellow, IEEEOptical Signal Processor for Millimeter-Wave Interferometric Radiometry

[7] E.Nova (2015) Millimeter Wave and Terahertz Imaging Techniques

[8] I. Corbella , N. Duffo , M. Vall-llossera , A. Camps , F. Torres. The visibility function in interferometric aperture synthesis radiometry (2004)

[9] Adriano Camps, Ignasi Corbella, Javier Bara, and Francesc Torres. Radiometric Sensitivity Computation in Aperture Synthesis Interferometric Radiometry (1998)

[10] Paul M. Blanchard, Alan H. Greenaway, Rupert N. Anderton, and Roger Appleby. Phase calibration of arrays at optical and millimeter wavelengths

[11] Alexandre Mottet, Nicolas Bourriot, Jérôme Hauden. Tunable Frequency Shifter Based on LiNbO3- I&Q Modulators

[12] A.Camps (1996) Application of interferometric Radiometry to Earth Observation

[13] Yuntao,Yuesong Jiang, Yuedong Zhang, and Guoli Fan Study of terahertz interferometric imaging using optical techniques

[14] Juan Wei, Fangzheng Zhang, Yonggang Zhou, De Ben, and Shilong Pan. Stable fiber delivery of radio-frequency signal based on passive phase correction

[15] Shouyuan Shi, Chris Schuetz, Rick Martin, Tom Dillon, Peng Yao, Janusz Murakowski, Garrett Schneider, and Dennis W. Prather. System Modeling of Passive Millimeter Wave

Imager Based on Optical Up-conversion

[16] Yuedong Zhang, Yuesong Jiang, Jingping Guo, Yuntao He, Haiyang Wang. Application of millimeter-wave photonics technology in passive millimeter-wave imaging

[17] Richard Martina, Christopher A. Schuetza, Thomas E. Dillona, Caihua Chenb, Jesse Samlukb, E. Lee Stein Jr. b, Mark Mirotznikc, and Dennis W. Prather. Phase Sensitive Innovations Inc., 51 East Design and Performance of a Distributed Aperture Millimeter-Wave Imaging System using Optical Upconversion

[14] Christopher Schuetzc, Richard Martina, Thomas Dillona, Peng Yaoa, Daniel Mackridesa, Charles Harritya, Alicia Zablockia, Kevin Shrevea, James Bonnettb, Petersen Curtb, and Dennis Pratherc Realization of a Video-Rate Distributed Aperture Millimeter-Wave Imaging System using Optical Upconversion

[18] Graham H. Smith, Student Member, IEEE, Dalma Novak, Member, IEEE, and Zaheer Ahmed. Overcoming Chromatic-Dispersion Effects in Fiber-Wireless Systems Incorporating External Modulators